The Equilibrium Line Altitude of isolated glaciers during the Last Glacial Maximum – New insights from the geomorphological record of the Monte Cavallo Group (south-eastern European Alps)

Lukas Rettig [a, *], Giovanni Monegato [b], Matteo Spagnolo [c], Irka Hajdas [d], Paolo Mozzi [a]

[*] Corresponding author (lukas.rettig@phd.unipd.it)

[a] Department of Geosciences, University of Padua, Via G. Gradenigo 6, 35131 Padova, Italy

[b] Institute of Geosciences and Earth Resources, National Research Council, Via G. Gradenigo 6, 35131 Padova, Italy

[c] School of Geosciences, University of Aberdeen, Elphinstone Road, AB243UF Aberdeen, United Kingdom

[d] Laboratory of Ion Beam Physics, ETH Zürich, Otto-Stern-Weg 5, 8093 Zürich, Switzerland

Abstract: Glacier-based reconstructions of Equilibrium Line Altitudes (ELAs) are important to understand changes of temperature and precipitation over longer time scales and may help to validate regional palaeoclimate models. Here, we present new insights into the ELA in the south-eastern part of the European Alps during the Last Glacial Maximum (LGM, 26.5 to 19 ka), based on the geomorphological record of the Monte Cavallo Group (Venetian Prealps, NE-Italy). This mountain range hosted a glacial system that remained isolated from larger valley glaciers in its vicinity and therefore likely responded very dynamically to changes in climatic boundary conditions. Through detailed mapping of glacial sediments and landforms, we were able to constrain the extent of these palaeoglaciers and model their surface geometry and ELA via semi-automated toolboxes in a geographic information system. In the absence of numerical datings, these landforms were related to an LGM advance through geomorphological and stratigraphical means. In a next step, ELAs were also recalculated for other LGM glaciers in the south-eastern Alps, allowing wider palaeoclimatic conclusions to be drawn. These ELAs are in the range of 1100 to almost 1700 m and show a strong E-W gradient with particular low values in the Julian and eastern Carnic Prealps. This pattern indicates that during the LGM a precipitation gradient existed along the south-eastern fringe of the Alps, with moisture being preferentially advected to these mountain ranges while the Venetian Prealps in the West received less precipitation. Based on the reconstructed ELAs, annual precipitation sums during the regional LGM glacier culmination (ca. 25.5 to 23.5 ka) are estimated between 1820 and 2920 ± 750 mm/yr. Those values are largely compatible with data from modern weather stations and indicate no or little reduction in LGM precipitation as it is reported from other parts of the Alps.

Keywords: Equilibrium Line Altitude, Glacial geomorphology, Geomorphological mapping, Palaeoclimate, Radiocarbon dating

1. Introduction

Glacial landforms and deposits are suitable proxies of the palaeoclimate since changes in the Equilibrium Line Altitudes (ELAs) of mountain glaciers primarily reflect fluctuations in air temperature and precipitation (Ohmura et al., 1992; Ohmura and Boettcher, 2018). In mountainous regions, such as the European Alps, the reconstruction of palaeo-ELAs in selected areas is therefore a key element to better understand the interactions between the atmosphere and the cryosphere over longer time scales (e.g., Kerschner and Ivy-Ochs, 2008; Rea et al., 2020). Specifically, reconstructed ELAs can be used to quantitatively determine palaeoprecipitation, assuming an independent proxy for palaeotemperature is available (Spagnolo and Ribolini, 2019; Rea et al., 2020). This is of particular importance for the Last Glacial Maximum (LGM), for which little quantitative information on palaeoprecipitation is available. Globally, the LGM is defined as the period between 26.5 and 19 ka (from hereon: “global LGM”), which was characterised by a lowstand in sea-level and a maximum expansion of the Earth’s ice sheets (Clark et al., 2009). ELAs of LGM glaciers have been calculated in a few sectors of the Alps on the basis of geomorphological evidence, sometimes combined with numerical dating methods (Forno et al., 2010; Federici et al., 2012; Monegato, 2012; Bernsteiner et al., 2021; Rettig et al., 2021). For many areas, however, data is still sparse and further investigations are necessary both to gain better insights into the evolution of these glaciers and to test the performance of Alpine-scale palaeoclimate models that have recently been presented (Višnjević et al., 2020; Del Gobbo et al., 2022).

During the global LGM, the European Alps were covered by a complex glacier network, which comprised local ice domes in the central Alps (Florineth and Schlüchter, 2000; Kelly et al., 2004) that fed large outlet glaciers on both sides of the mountain range (Monegato et al., 2007; Reber et al., 2014; Gianotti et al., 2015; Monegato et al., 2017; Ivy-Ochs et al., 2018; Braakhekke et al., 2020; Kamleitner et al., 2022). Recent advances in ice sheet and palaeoclimate modelling have significantly improved our understanding of the extent and dynamics of the Alpine palaeoglacier network, and the climatic conditions under which it evolved (Kuhlemann et al., 2008; Seguinot et al., 2018; Višnjević et al., 2020; Del Gobbo et al., 2022). Combined with proxy records from cave speleothems, such models point to an increased moisture supply during the global LGM from the Mediterranean Sea, following a southward shift of the North Atlantic jet stream (Florineth and Schlüchter, 2000; Luetscher et al., 2015; Spötl et al. 2021). This resulted in generally depressed ELAs in the Mediterranean mountains (Kuhlemann et al., 2009; Hughes et al., 2010; Baroni et al., 2018; Allard et al., 2020) and across parts of the southern Alps, allowing glaciers in these areas to expand even in catchments with lower elevations (Monegato et al., 2007; Del Gobbo et al., 2022). However, it remains difficult to accurately model the surface geometry and ELA of large and interconnected LGM glacial systems (Ehlers and Gibbard, 2004; Seguinot et al., 2018). Additionally, these glaciers often had large catchments, in which climatic conditions may have substantially varied between accumulation and ablation areas. As a result, variations in ELA over smaller spatial scales or local precipitation gradients during the LGM have remained poorly constrained.

Smaller, isolated valley glaciers and ice caps, on the other hand, represent more direct proxies of the local palaeoclimate and they probably reacted more quickly to climatic changes (Reuther et al., 2011). If sufficiently constrained by geomorphological evidence (i.e., frontal and lateral moraine ridges), it is possible to reconstruct their three-dimensional geometries, to calculate their ELAs and to ultimately quantify palaeoclimatic parameters. Several of these isolated glaciers developed along the south-eastern fringe of the Alps in the mountain ranges of the Venetian, Carnic, and Julian Prealps (NE-Italy). Their geomorphological record has been described in a few areas, both through geological mapping campaigns (Barbieri & Grandesso, 2007; Zanferrari et al., 2013) and through studies that specifically aimed at reconstructing former ice extents and ELAs (Fuchs, 1970; Carraro and Sauro, 1979; Baratto et al., 2003; Monegato, 2012; Rettig et al., 2021). However, only few of these studies have applied numerical approaches (Benn and Hulton, 2010; Pellitero et al., 2016) to acquire palaeoglacier geometries, and the reported ELAs were calculated using different methods (including the Accumulation-Area-Ratio (AAR), Area-Altitude Balance Ratio and Toe to Headwall Altitude Ratio (THAR) methods), thus making a potential comparison at a regional scale unreliable. Additionally, no numerical datings have yet been reported from isolated glaciers in the south-eastern Alps, partially due to the difficulty of applying surface exposure dating in carbonate catchments (cf. Žebre et al., 2019). The outermost moraines in these mountain ranges have therefore been ascribed to a local LGM advance only through stratigraphical and geomorphological means, highlighting the need for a more systematic comparison between sites to strengthen the regional relative chronology.

The extent of the local LGM is still debated at a few key sites, one of which is the Monte Cavallo Group (MCG), in the eastern part of the Venetian Prealps. Located extremely close to the Alpine fringe, palaeoglaciers in this mountain range were likely strongly dependent on southerly-derived moisture, making it an ideal study site to better understand LGM palaeoprecipitation patterns. Here, we present new data concerning the glacial geomorphology of the MCG with the aim to reconstruct the extent of palaeoglaciers during the local LGM and to calculate their ELAs. In a next step, ELAs are also recalculated for a few LGM palaeoglaciers in other parts of the south-eastern Alps, based on the geomorphological evidence presented in earlier studies but applying a methodologically consistent framework based on numerical approaches (Pellitero et al., 2015, 2016). This enables us to compare our results with modern day climatic patterns, as well as with models of ELAs and palaeoclimate during the LGM on a wider Alpine scale.

2. Regional setting

2.1. The south-eastern European Alps during the LGM

The south-eastern sector of the European Alps encompasses the mountain ranges of the Venetian, Carnic, and Julian Prealps, located in the Italian regions of Veneto and Friuli Venezia Giulia (Fig. 1a). Here, the Alpine fringe follows an approximate SW-NE direction, similar to that of the shoreline of the Adriatic Sea that is at a distance of ca. 60 to 80 km. The pre-Alpine mountains are characterised by relatively low elevations with the highest peaks reaching elevations between 2000 and 2500 m a.s.l. They are cut by a series of transverse valleys that drain the mountainous catchments towards the Venetian and Friulian plains in the South. Presently, the most important fluvial systems are the Adige, Brenta, Piave and Tagliamento rivers and their tributaries.

The climate in the south-eastern Alps is strongly influenced by both their position at the southern margin of the mountain range and their proximity to the Adriatic Sea. Mean annual precipitation (MAP) is among the highest in the whole Alpine region (Isotta et al., 2014; Crespi et al., 2018). At Monte Canin, in the Julian Alps, for instance, a MAP of 3335 mm/yr has been reconstructed for the period between 1981 and 2010 (Culucci and Guglielmin, 2015). Much of this is provided by intense rainfall events that occur most often during the spring and autumn seasons (Isotta et al., 2014). Such high precipitation has up until today allowed small glaciers and firn patches to persist at relatively low elevations, despite rising temperatures during the last decades (Colucci et al., 2021). Moving towards the Venetian Prealps in the West, however, a clear decrease in MAP down to 1400-1600 mm/yr can be noted (Isotta et al., 2014; Crespi et al., 2018; see Fig. 1b).

During the global LGM, the higher catchments of the south-eastern Alps represented accumulation areas for large glaciers that occupied the main valleys and were occasionally interconnected through transfluences over low-elevated saddles (Castiglioni, 1940; Pellegrini et al., 2005; Monegato et al., 2007; Rossato et al., 2013; Monegato et al., 2017; Rossato et al., 2018). At their maximum extent, some of these glaciers advanced beyond the Alpine front, depositing prominent morainic amphitheatres in the foreland plains (Fig. 1c). The regional chronology of the LGM ice advance was established in several studies through geomorphological and stratigraphical investigations of these moraine records, coupled with Accelerator mass spectrometry (AMS) radiocarbon dating. Those studies show that the maximum glacier extent corresponds to the period of the global LGM during Marine Isotope Stage (MIS) 2. For the Tagliamento glacier, a two-fold LGM advance with a first pulse between 26.5 and 24 cal ka BP, and a second between 22 and 21 cal ka BP has been reconstructed (Monegato et al., 2007). The Garda glacier reached its maximum extent slightly later, just after 24.9 cal ka BP, but remained at a sustained frontal position until its collapse between 17.7 and 17.3 cal ka BP (Ravazzi et al., 2014; Monegato et al., 2017). The LGM chronology of the Piave glacier is somewhat less well constrained, but the last advance in the amphitheatre of Vittorio Veneto is dated to between 21.6 and 20.6 cal ka BP (Bondesan et al., 2002). With the combined chronologies of the Garda and Tagliamento amphitheatres (see Fig. 2), two phases of regional glacier culmination in the south-eastern Alps can be defined: A first phase between ca. 25.5 and 23.5 ka (from hereon: “early regional LGM advance”) and a second phase between ca. 23 and 21 ka (from hereon: “late regional LGM advance”). These dates also coincide with a period of high aggradation in related alluvial fans and megafans in the Venetian and Friulian plains between 26 and 19 cal ka BP, providing independent age control for the regional LGM chronology (e.g., Carton et al., 2009; Fontana et al., 2014; Rossato and Mozzi, 2016).

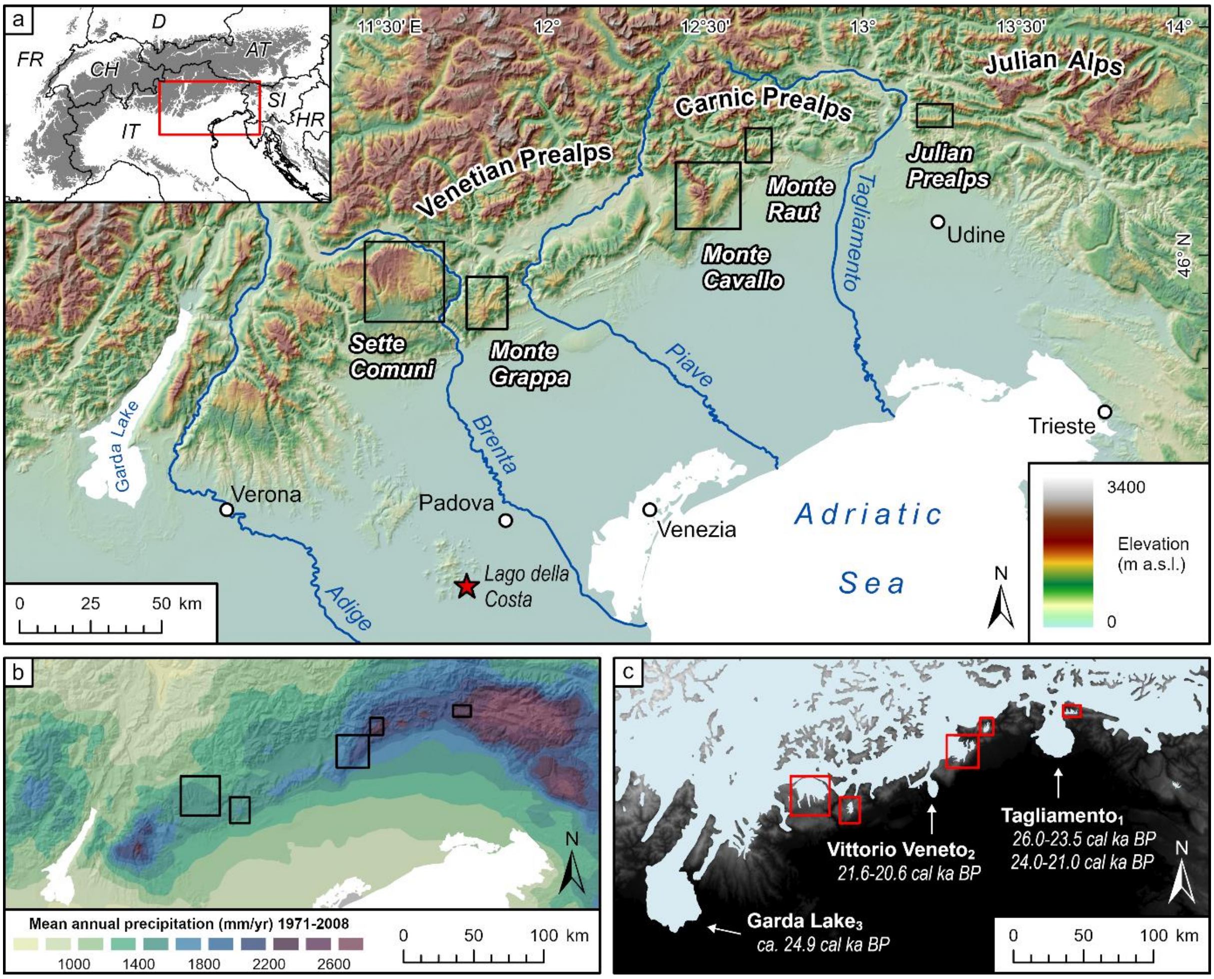

Fig. 1. a. Topographic map of the south-eastern fringe of the European Alps, showing the locations of mountain ranges that are subject to this study. **b.** Mean Annual Precipitation (MAP) in the south-eastern Alps during the period 1971-2008, digitised from the dataset of Isotta et al. (2014). The locations of the study areas are also shown for reference. Note especially high MAP in the eastern Carnic and Julian Prealps. **c.** Glacier extent in the south-eastern Alps during the LGM. Glacier outlines were updated from Ehlers and Gibbard (2004) and radiocarbon ages for glacial advances taken from (1) Monegato et al. (2007), (2) Bondesan et al. (2002), and (3) Monegato et al. (2017). Underlying elevation data for all figures: EU-DEM v1.1. (*land.copernicus.eu*).

The fringe of the pre-Alpine mountains hosted smaller glaciers that even at their local LGM remained isolated from the large systems. In the Julian Prealps, for instance, several valley glaciers developed along the northern slopes of the Chiampon – Cuel di Lanis ridge (Monegato, 2012; Zanferrari et al., 2013). Around 40 km farther west, in the Carnic Prealps, the limestone plateaus of the Monte Raut served as accumulation areas for glaciers advancing northwards into the Silisia Valley (Rettig et al., 2021). The Monte Grappa (Venetian Prealps) hosted a more complex glacial system that probably comprised a local ice cap with outlet glaciers extending into the valleys towards north, west, and south (Carraro and Sauro, 1979; Baratto et al., 2003). The largest pre-Alpine glacier developed on the Sette Comuni plateau, leaving extensive geomorphological evidence, such as the frontal moraine ridges at the town of Asiago (Barbieri and Grandesso, 2007). Isolated glaciers probably also existed in other areas, such as along the western slope of the Monte Baldo, or on parts of the Lessini Plateau (e.g., Pasa, 1940; Sauro, 1973; Mattana, 1974), but due to the absence or ambiguity of the geomorphological evidence, these areas will not be addressed in further detail here.

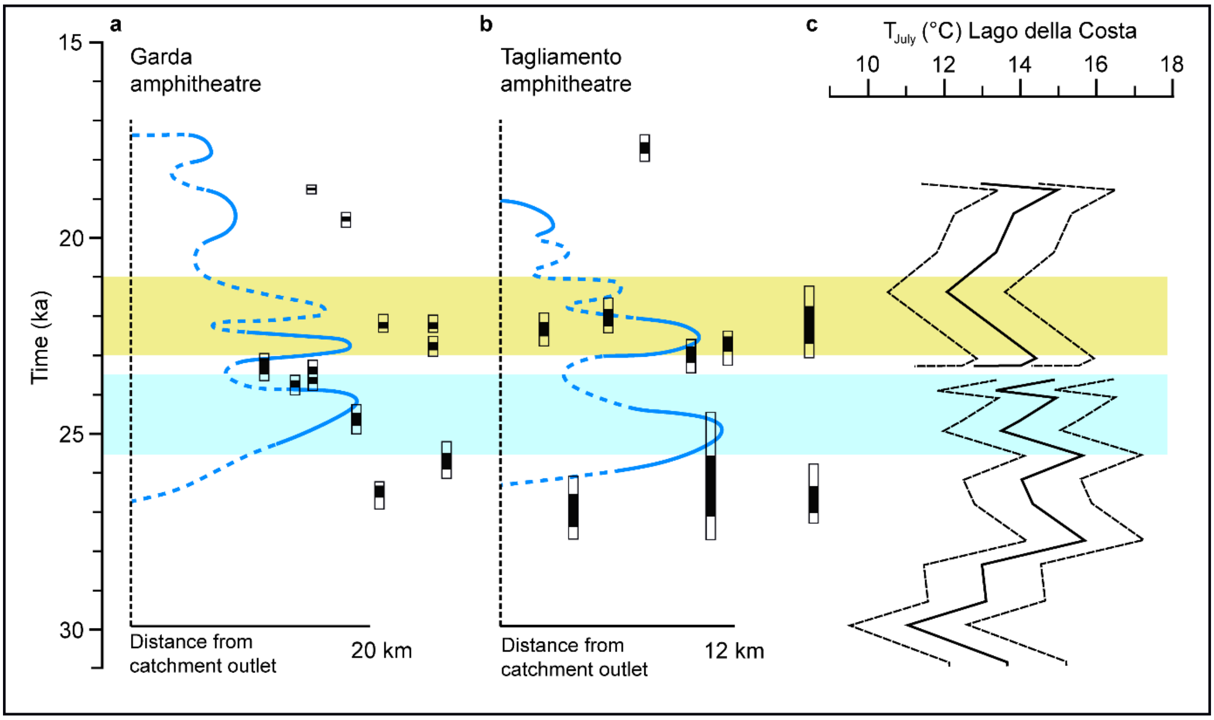

Fig. 2. Frontal fluctuations of the (**a**) Garda and (**b**) Tagliamento outlet glaciers during the global LGM (redrawn from Kamleitner et al., 2022). Calibrated radiocarbon ages from Monegato et al. 2017 (Garda) and Monegato et al. 2007 (Tagliamento) are indicated by solid (68.2% probability range) and transparent (95.4% probability range) bars. From the combined records of these glaciers, two periods of regional glacier culmination can be defined, a first during the early LGM (light blue box, ca. 25.5 to 23.5 ka) and a second during the late LGM (yellow box, ca. 23 to 21 ka). **c.** Reconstructed July temperatures during the global LGM, from the chironomid record at Lago della Costa (redrawn from Samartin et al., 2016). The dashed lines represent the sample-specific error of prediction of the reconstruction (ca. ± 1.55°C).

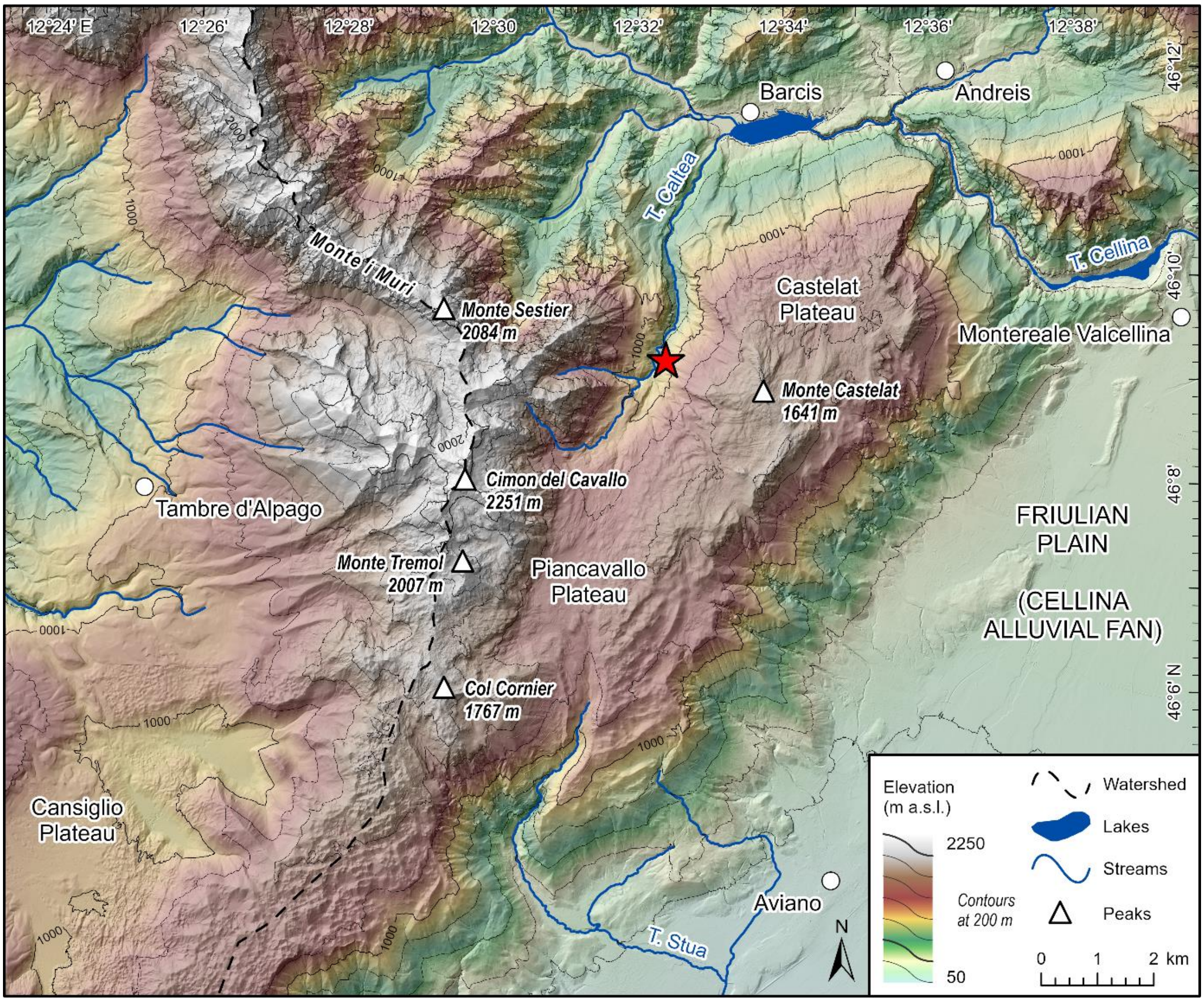

Fig. 3. Topographic map of the MCG. Note the particular relief of the area with plateaus around 1000 to 1500 m and a higher elevated part around Cimon del Cavallo (2251 m). The red star indicates the location of the lacustrine section in the Caltea Valley (cf. Fig. 7). Underlying elevation data: FVG-DEM (*eaglefvg.regione.fvg.it*).

2.2. Outline of the Monte Cavallo Group

The MCG represents the easternmost extent of the Venetian Prealps and separates the Piave catchment, to the West, from the Cellina catchment, to the North and East (Fig. 3). While the Cellina Valley is characterised by steep and narrow slopes, the western side of the MCG, around the basin of Alpago, shows more gentle morphologies that have been shaped by Pleistocene activity of the large Piave Glacier (Pellegrini et al., 2005). At its south-eastern foot, the MCG is delimitated by the Cellina alluvial fan (Avigliano et al., 2002). The MCG comprises several karst plateaus at elevations between ca. 1000 and 1500 m, which are, from SW to NE: the

Cansiglio Plateau, the Piancavallo Plateau and the Castelat Plateau. Towards the Northwest, the relief becomes steeper with its highest peak, the Cimon del Cavallo, reaching an elevation of 2251 m. There are two major valleys that cut through the MCG: The Caltea Valley follows a northwards direction towards Barcis and the Cellina River, and the Stua Valley, which first trends southwards and then, after an eastward turn, towards the Friulian plain.

The bedrock comprises a succession of Mesozoic to Cenozoic sedimentary units that were stacked and folded during the Alpine orogeny (Cancian et al., 1985; Carulli et al., 2006). The oldest strata are Triassic dolostones (*Dolomia Principale Formation*) that crop out in the northern parts of the study area. They are overlain by Jurassic and Cretaceous limestones that occur both in slope or basin and in platform facies (*Cellina Formation* and *Monte Cavallo Formation*). These latter units cover the largest part of the study area and are subject to strong karstification as indicated by the widespread presence of epigenic karst features such as karren, shafts, dolines, and an extensive cave system underneath the Cansiglio Plateau (Castiglioni, 1964; Vincenzi et al., 2011). Younger, Cenozoic formations crop out more sporadically and are concentrated in the Alpago Basin and the foothills along the plain. Some patches of these units, including conglomerates, siltstones, and arenites, can also be found along parts of the Caltea Valley.

The presence of glacial sediments and landforms in the MCG has been recognised since at least the second half of the 19th century, but the extent of the palaeoglacier network during the local LGM and its relation to the larger Alpine outlet glaciers have been since subject to debate. Taramelli (1875) postulated that a glacier tongue flowing down the Caltea Valley merged with the larger Cellina Glacier around Barcis. A similar interpretation was also presented in Ehlers and Gibbard (2004). According to Penck and Brückner (1909) and Castiglioni (1940), on the other hand, the Cellina Valley remained ice-free throughout the Pleistocene glaciations, allowing the Caltea Glacier to retain its independent dynamics. A more detailed overview of the glacial geomorphology of the MCG is presented by Fuchs (1970), who also calculated a first ELA (1350 m) for the LGM palaeoglaciers. This value represents an average between the elevation of Cimon del Cavallo (2251 m), the highest peak in the catchment, and the lowermost position of moraines in the Caltea Valley (450 m), a method known as the Toe-to-Summit Altitude Ratio (Benn and Lehmkuhl, 2000). Fuchs (1969) also presented chronological control for the onset of glaciation in the area (29,350 ± 460 ^{14}C yr BP) from a lacustrine succession in the Caltea Valley that is covered by till from the ultimate glacier advance. Since these studies, however, no systematic investigations concerning the glacial history of the MCG have been conducted, nor was a more sophisticated and reliable palaeoglacier reconstruction and ELA calculation attempted.

3. Methods

3.1. Geomorphological mapping

The geomorphological survey of the MCG was performed through a combination of mapping from remotely sensed datasets and field assessments (cf. Smith et al., 2006; Chandler et al., 2018), with a focus on identifying deposits and landforms of glacial origin that could be used to constrain the limits of the palaeoglacier network. Remotely sensed data were derived from the geoportals of Regione Friuli Venezia Giulia (*https://eaglefvg.regione.fvg.it/*) and Regione Veneto (*https://idt2.regione.veneto.it/*) and integrated into a geographic information system (GIS) environment (*Esri ArcGIS Pro 2.9*). The data included topographic maps at a scale of 1:5000 (Carta Tecnica Regionale), panchromatic orthophotos at a ground resolution of 10 cm and, for the Friulian part of the study area, also recently-acquired LIDAR data (Sample density: 4 points/m^2, Sampling time: 2006-2010). Field surveys were then carried out in selected areas for ground-truthing of the geomorphological mapping. This was particularly necessary to accurately represent smaller landforms and glacial deposits that were not visible on the topographic maps, the orthophotos, or the DEM. Additionally, Quaternary deposits were described in the field according to their sedimentary properties, such as grain size, clast shape, lithology, or bedding structures, to assess their origin (Evans and Benn, 2021). In the absence of numerical datings, special attention was paid to morphological and sedimentological indicators of relative ages of moraine ridges and glacial deposits, including colours (via Munsell colour chart), development of soils and degree of cementation (e.g., Burke and Birkeland, 1979; Colman and Pierce, 1986; Lukas, 2006). These properties were then compared to regional maps and descriptions of soils on glacial deposits for which numerical data are available (cf. Provincia di Treviso and ARPAV, 2008). This was necessary to evaluate if the investigated moraines indeed correspond to glacier advances during the global LGM or if they potentially pertain to older glaciations.

3.2. Radiocarbon dating

A section of lacustrine deposits in the upper Caltea Valley (cf. Fuchs, 1969) was revisited with the aim to obtain new chronological control on these sediments through AMS radiocarbon dating. These lacustrine deposits are covered by glacial till from the ultimate glacier advance and therefore the idea was to use this section to predate the onset of the local LGM. A total of ten organic macrofossils were collected from the section including twigs, branches, and pieces of bark that were buried within the lake sediments (see section 4.1.3. for details). After sampling, the material was dried at 40°C for 24 hours and then chemically treated according to standardised methods to remove any potential contamination from carbonates or humic acids (Hajdas, 2008). Samples were subsequently graphitised and measured in the AMS radiocarbon system (MICADAS) at the Laboratory of Ion Beam Physics at ETH Zurich, Switzerland (Synal et al., 2007).

3.3. Palaeoglacier and ELA reconstructions

Reconstructions of palaeoglacier 3D surfaces were carried out using the semi-automated GIS toolbox "GlaRe" developed by Pellitero et al. (2016). This toolbox calculates the thickness of a former glacier along user-defined flowlines, assuming perfectly plastic ice rheology (Nye, 1952; Schilling and Hollin, 1981; Benn and Hulton, 2010). The flowlines were manually digitised following the thalweg of the major valleys and according to ice-flow directions indicated on glacially moulded bedrock. The model was spatially constrained by mapped landforms indicating frontal and lateral glacial limits. In a first modelling step, shear stress along the flowlines was set to 100 kPa (Pellitero et al., 2016) and then partially adjusted so that the reconstructed ice thickness better matched the geomorphological evidence, in particular the elevation of lateral moraine ridges. Where glaciers were topographically constrained, an F-factor correction was applied to account for lateral drag exerted by the valley walls (Nye, 1965; Benn and Hulton, 2010). Owing to the complexity of the glacier network with multiple outlets, ice thickness had to be modelled separately along several flowlines before the 3D glacier surface could be interpolated across the entire area. The uncertainties in this approach are largely connected to the quality of the geomorphological evidence that constrains the model. In areas where such evidence was weak (e.g., where frontal moraines were lacking), the glacier modelling was repetitively applied with hypothetical glacier fronts to check which frontal position would best correlate with observed lateral glacier limits.

In some parts of the Caltea and Stua valleys, a first modelling attempt yielded ice surfaces that were too low when compared to the elevation of lateral moraines, even if high shear stresses were applied. We concluded that in these areas there had been substantial post-LGM fluvial erosion of the valley floor, enhanced by tectonic fracturing of the underlying bedrock along a major fault line. As a result, the present-day topography does not correctly resemble that of the former subglacial bed. To overcome this problem, we manually filled these parts of the DEM by interpolating between the scarps of fluvial erosion on both sides of the valleys. This resulted in a modified DEM which was up to 80 m higher than the current valley bottom. A remodelling of the ice surface based on this modified DEM yielded more adequate results.

In a next step, ELAs were calculated from the reconstructed glacier surfaces, using a separate toolbox (Pellitero et al., 2015). Different techniques of ELA reconstruction were applied: For the Area-Altitude-Balance-Ratio (AABR) method (Furbish and Andrews, 1984; Osmaston, 2005; Rea, 2009), a balance ratio of 1.56 was chosen, as this represents a median value for modern glaciers worldwide (Oien et al., 2022). Additionally, the application of a regional AABR (1.29 for the European Alps; Oien et al., 2022) was tested, although it is debatable if such regional correlations are valid for Pleistocene settings as well. ELAs were also calculated via the Accumulation-Area-Ratio (AAR) method, to enable a more direct comparison with those that have been determined in other parts of the Alps through this technique (e.g., Forno et al., 2010). AARs of 0.58 (global median, Oien et al., 2022) and 0.67 (European Alps, Gross et al., 1977) were used. The results of the AABR- and AAR-methods were further compared with independent geomorphological evidence such as the Maximum Elevation of Lateral Moraines that often corresponds to the ELA (MELM, Lichtenecker, 1938).

3.4. Reconstructing palaeoglacier geometries and ELAs of LGM glaciers in other parts of the south-eastern Alps

ELAs of LGM palaeoglaciers have been frequently reported from other mountain ranges of the south-eastern Alps (cf. section 2.1.). Since they have been acquired through different methods of palaeoglacier and ELA reconstruction, however, more quantitative comparisons among sites have been difficult to achieve so far. To overcome this problem, we recalculated palaeoglacier 3D geometries and ELAs for a few key sites based on the geomorphological evidence presented in the original publications but applying a methodologically consistent framework similar to that used for reconstructing glaciers in the MCG (Pellitero et al., 2015, 2016). Shear stress values and F-factor correction were adjusted at each site to match the existing morphological evidence presented in the publications or maps. The sites were chosen to represent a W-E transect through the pre-Alpine mountains and limited to those areas where robust geomorphological information was available from previous studies or mapping campaigns. They include three valley glaciers (Vodizza, Bombasine, and Pozzus) in the Julian Prealps (Monegato, 2012; Zanferrari et al., 2013), the ice cap of Monte Grappa (Carraro and Sauro, 1979; Baratto et al., 2003), and the plateau glacier of Sette Comuni (Barbieri & Grandesso, 2007). For the Monte Raut, numerically reconstructed ELAs applying the same approach have recently been reported (Rettig et al., 2021), so the results from this study were integrated into the wider discussion. The locations of these glaciers are reported in Fig. 1 and some general introduction into the setting is given in section 2.1. For further details regarding the geomorphological evidence, we refer to the original publications or maps.

3.5. Quantifying palaeoprecipitation

Reconstructed ELAs in the MCG and other areas of the south-eastern Alps were used as an input for quantifying palaeoprecipitation, as frequently applied in palaeoglacier studies in the Alps and elsewhere (e.g., Benn and Ballantyne 2005; Chandler et al., 2019; Spagnolo and Ribolini, 2019). These quantitative estimates are possible if independent information on summer temperatures is available from other proxy records, such as chironomid assemblages, and by using empirical P/T relationships, determined from datasets of modern glaciers (e.g., Ohmura et al., 1992; Ohmura and Boettcher, 2018):

$$P = 5.87\ T_{Melt}^2 + 230\ T_{Melt} + 966 \qquad \text{(Eq. 1)}$$

Here, P is the annual precipitation (mm/yr) and T_{Melt} is the mean atmospheric temperature (°C) of the summer months (Northern Hemisphere: June, July, and August) at the ELA. While for a long time independent temperature estimates for the global LGM were not available in the greater Alpine region, a chironomid record covering the period between 31 and 17 cal ka BP was recently presented from Lago della Costa in the Euganean Hills (7 m a.s.l.; Samartin et al., 2016), located ca. 60 km south of the alpine margin and 110 km to the Monte Cavallo, respectively. The chironomid assemblages at this site indicate that July temperatures (T_J) were on average around 14.3°C (corresponding to a temperature difference of 8.7°C to the period 1961-1990) during the early regional LGM advance between 25.5 and 23.5 ka (Fig. 2). Slightly colder temperatures are recorded for the late regional LGM advance (23 to 21 ka), averaging at 13.2°C and reaching a minimum of 12.1°C at 21.4 cal ka BP (Samartin et al., 2016).

Due to the absence of precise chronological control, we have decided to calculate palaeoprecipitation based on the average temperatures for these two time periods. We have preferred to use averages over minima since the prominent morphologies of the moraine ridges suggest that they have been formed during a sustained period of climatic cooling rather than during a short-lived glacier advance. For simplicity, T_J at Lago della Costa was assumed to represent T_{Melt} and was then extrapolated to the respective glacier ELAs using an altitudinal temperature lapse rate of 6.5°C km^{-1}. This lapse rate is most commonly applied in paleoclimate studies in the Alps (e.g., Spagnolo and Ribolini, 2019; Ribolini et al., 2022), even though actual LGM lapse rates may have varied from this estimate. Summer temperatures at the ELA were ultimately translated to palaeoprecipitation using Eq. 1.

Quantitative reconstructions of palaeoprecipitation from ELAs are not straightforward and are related to a number of uncertainties. We have aimed to quantify these uncertainties in our calculations by propagating the errors related to (1) the reconstruction of the ELA from the 3D glacier surface using average AABR- and AAR-values determined from a set of modern glaciers worldwide; (2) the reconstruction of July temperatures at Lago della Costa from the chironomid record; and (3) the relationship between summer temperature and annual precipitation at the ELA. For (1) the median difference between calculated and measured ELAs is 65.5 m (Oien et al., 2022); for (2) the error range is 1.55°C (Samartin et al., 2016) and for (3) the standard deviation is 648 mm/yr (Ohmura and Boettcher, 2018).

4. Results

4.1. Geomorphological and sedimentological evidence

Features that were used to reconstruct the geometry of the palaeoglacier network in the MCG comprise both (1) erosional landforms, such as glacial cirques or ice-moulded bedrock, that enabled the detection of former accumulation areas and ice-flow directions, and (2) depositional landforms and related sediments, primarily lateral and frontal moraine ridges, that constrain the spatial extent of the palaeoglaciers. These features are visualised in a geomorphological sketch map (Fig. 4).

4.1.1. Erosional features

Glacial cirques, representing source areas of former glaciation (Barr and Spagnolo, 2015), are located on both sides of the main crest of the MCG that stretches from Monte Tremol (2007 m) via Cimon del Cavallo (2251 m) towards Monte Sestier (2084 m) and the Monte i Muri chain (Fig. 5a, b). The cirques are partly over 1 km in diameter and framed by steep headwalls, the lower parts of which are frequently covered by talus and debris cones. Cirque floors are partially well-developed and usually situated at an elevation of around 1700 m. The bedrock in the cirques exhibits clear signs of ice-moulding such as smoothed surfaces and roche moutonnées, particularly visible in areas where ice was flowing over the cirque lips towards the Piancavallo Plateau and into the Caltea Valley. Glacial striae were not detected, possibly due to surface denudation of the soluble carbonate lithologies. Ice-moulded bedrock can also be found on some lower elevated plateaus, especially in the northern part of the Piancavallo Plateau (Pian delle More) and around Monte Castelat, suggesting that these areas were equally subject to glacial erosion. Remarkable features are also the deeply incised gorges in the lower Caltea and upper Stua valleys that point to enhanced fluvial erosion of the limestone bedrock by subglacial and/or proglacial meltwaters. Equally, several palaeo-channels lined with large boulders were found, indicating high water flow during the past. As such, they are in stark contrast to the present-day hydrology of the area, which is characterised by dominant subsurface drainage through aquifers in the karst system (Vincenzi et al., 2011; Filippini et al., 2018). Trimlines could not be detected with certainty in the MCG.

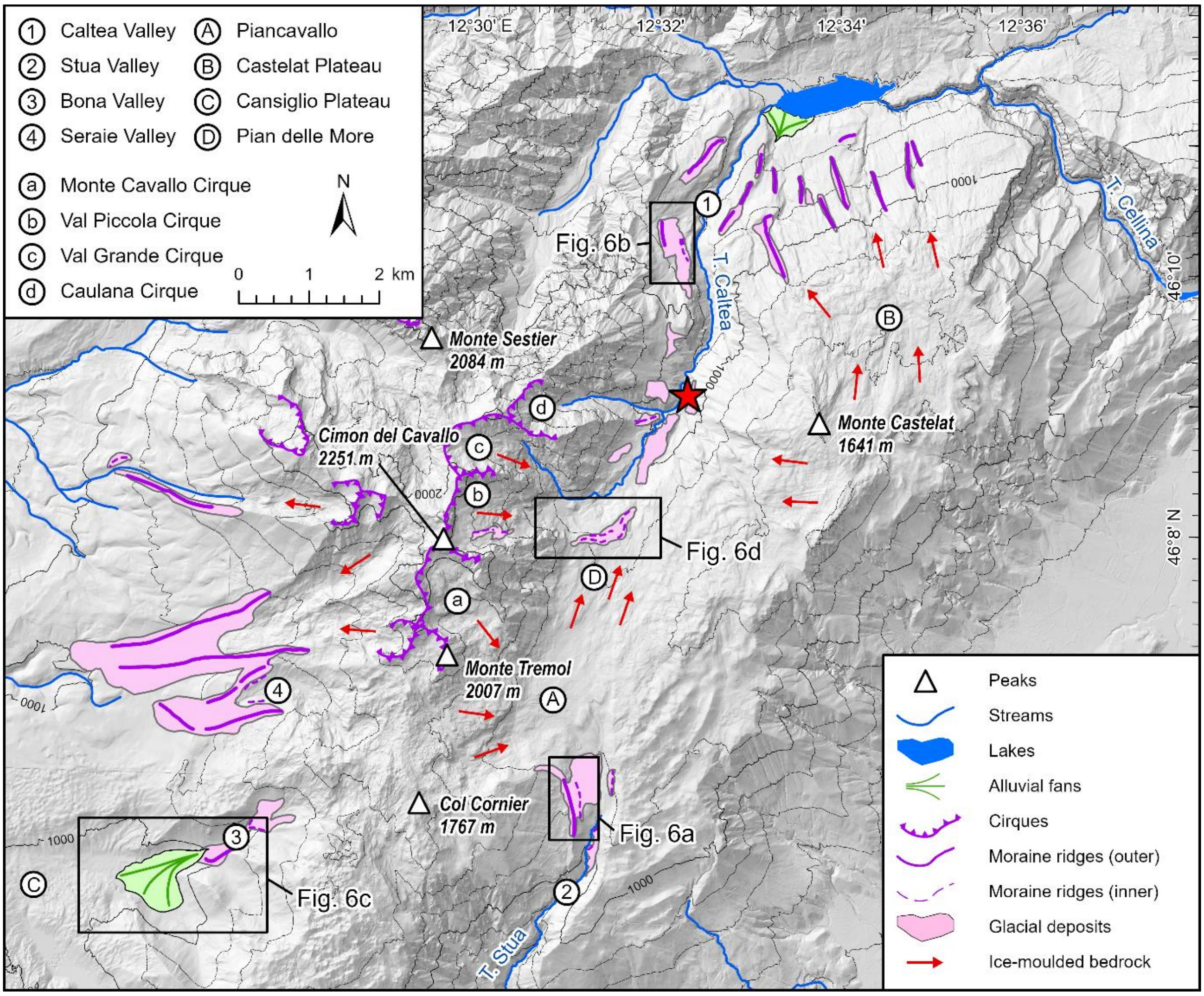

Fig. 4. Glacial geomorphological sketch map of erosional and depositional features in the MCG**.** Note that this sketch does not represent the entirety of landforms in the area, but its purpose is rather to visualise those that were used for glacier reconstructions. The red star indicates the location of the lacustrine section in the Caltea Valley (cf. Fig. 7). Underlying elevation data: FVG-DEM (*eaglefvg.regione.fvg.it*).

4.1.2. Depositional features

Evidence of glacial transport and deposition can predominantly be found in the lower sectors of the MCG, that represent former ablation areas. Large, glacially transported boulders occur in parts of the valley floors but are also spread throughout the Piancavallo Plateau, sometimes directly perched on top of the karstified bedrock (Fig. 5c). Frequently, outcrops of diamictic sediment can be found, which is characterised by a carbonate and predominantly silty matrix, incorporating edge-rounded and partially striated limestone clasts. In the lower parts of the Caltea Valley, also siltstone and arenite clasts are sometimes present within the diamicts, representing reworking of the locally outcropping Cenozoic bedrock. This enabled a clear distinction of glacially transported sediments with locally sourced deposits (e.g., of gravitational origin) that are always monogenic. In the valley bottoms, the diamicton is massive and exhibit a high degree of consolidation, which favours interpretation as a subglacial till (Evans et al., 2006). On the valley flanks, instead, they are oftentimes crudely stratified and sometimes intercalated with inclined gravel layers, reflecting deposition in an ice-marginal environment, typical of flow till (Fig. 5d). The sediments show only a limited degree of surficial weathering, and no cementation of the carbonate matrix was observed.

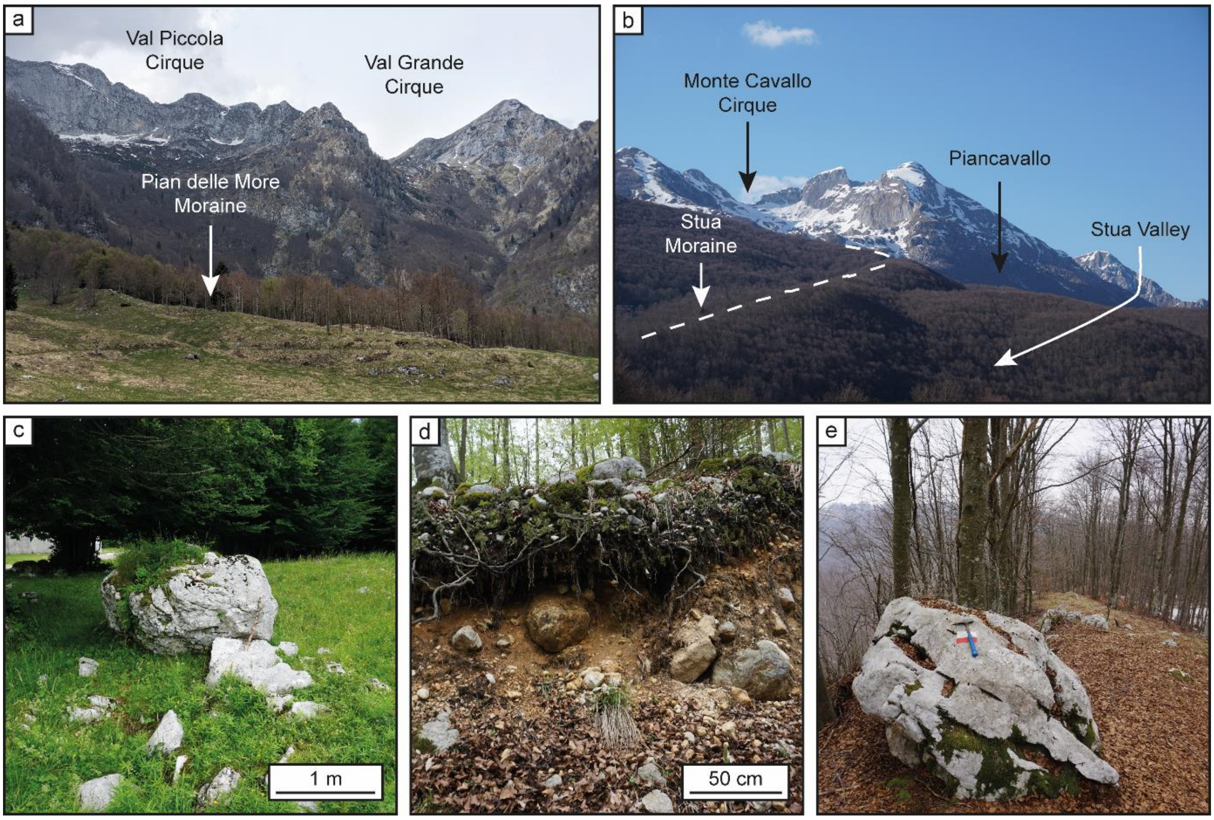

Fig. 5. Picture plate visualising geomorphological and sedimentological features of the glacial landscape **a.** The large cirques of Val Piccola and Val Grande as seen from Pian delle More. In the foreground, the prominent transverse moraine ridge can be seen (photograph taken on 04.05.2022). **b.** The upper part of the Stua Valley as seen from the road leading towards the Piancavallo Plateau. In the background, the Monte Cavallo Cirque is visible, from where ice was flowing over the plateau and into the valley. The extent of the glacier in the Stua Valley is well delineated by a prominent right lateral moraine (photograph taken on 08.04.2021). **c.** Large, glacially transported limestone boulder, perched on top of karstic bedrock in the northern part of the Piancavallo Plateau (photograph taken on 15.07.2021). **d.** Outcrop through a lateral moraine on the northern side of the Castelat Plateau, revealing crudely stratified diamict containing edge-rounded clasts (photograph taken on 05.06.2021). **e.** The crestline of the lateral moraine ridge in the Stua Valley, topped by a large limestone boulder. See hammer for scale (photograph taken on 04.03.2021).

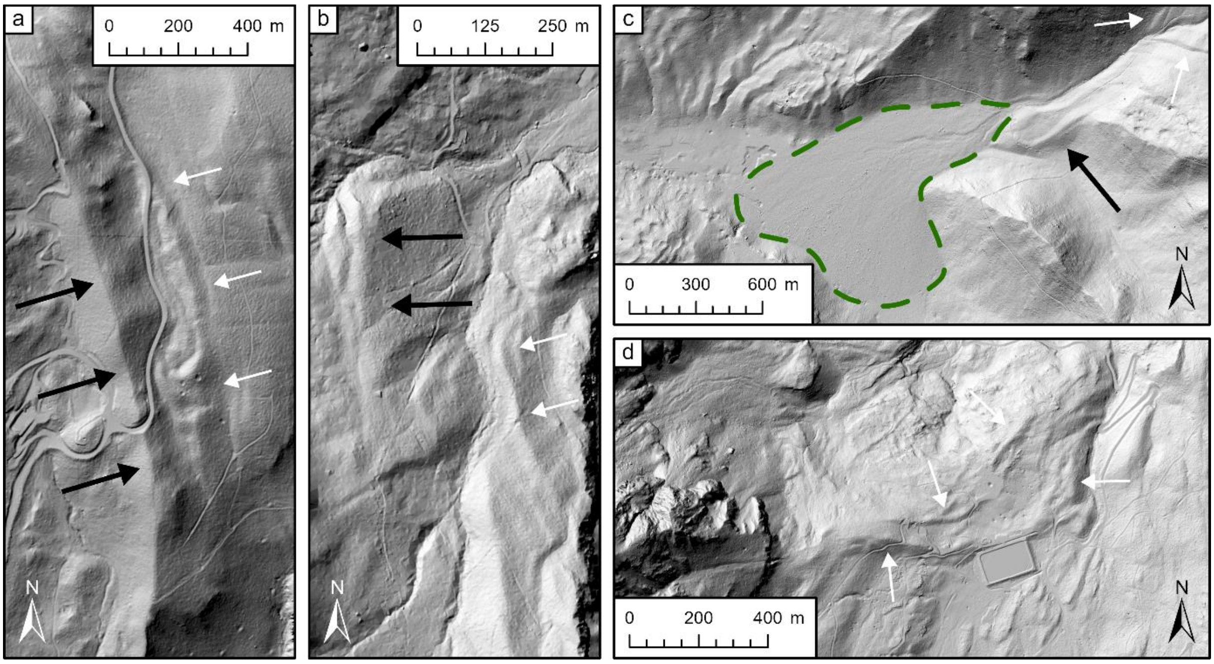

Fig. 6. Lateral and frontal moraine ridges in the MCG. The large outer moraines are indicated with bold black arrows, while the smaller, inner moraines are represented by white, thin ones. **a.** The upper Stua Valley with moraines preserved on the right side of the valley. **b.** The lower Caltea Valley with moraines preserved on the left side of the valley. **c.** The mouth of the Bona Valley. The green dashed line represents the extent of an alluvial fan that has been infilling the karstic polje. **d.** The transverse moraine ridges at Pian delle More. Underlying elevation data: FVG-DEM (eaglefvg.regione.fvg.it).

Lateral and frontal moraine ridges are the most common and prominent glacial landforms. In many valleys of the MCG, large, outer moraines can be morphologically distinguished from a second generation of smaller, inner ridges up-stream. The outer ridges often attain heights of over 20-30 m and their well-developed crestlines, dotted with large boulders (Fig. 5e), stretch for more than 1.5 km. The inner moraines, on the other hand, are typically more subdued and discontinuous and rarely exceed 5 m in height. This pattern is particularly apparent in the upper Stua Valley, where both generations of moraines are preserved on the right flank of the valley (Fig. 6a; cf. Fig. 5b). The frontal arcs of these moraines have mostly been eroded, but subglacial till is preserved along the valley bottom down to an elevation of ca. 950 m. In the Caltea Valley, moraines are preserved at lower elevations (down to ca. 600 m), which likely reflects both larger accumulation areas and a predominantly northerly exposure of the valley. Here, the frontal part of the outer moraine system has not been preserved entirely, but lateral moraines appear on both sides of the valley and the frontal position of the smaller, inner moraines can be identified (Fig. 6b). Moraine ridges can also be found in some valleys on the western side of the main divide. In the Seraie Valley, these moraines are particularly high (ca. 40 m) and stretch for more than 1.5 km down to an elevation of around 1100 m. In the Bona Valley, the frontal arc is preserved at an elevation of ca. 1020 m and connected to an alluvial fan that has been infilling a karstic Polje on the north-eastern edge of the Cansiglio Plateau (Fig. 6c). Smaller moraines delineate the northern edge of Pian delle More, representing right lateral moraines of a glacier coming from the Val Piccola Cirque (Fig. 6d, cf. Fig. 5a). Notable is that their crestlines are transverse to the direction of the Caltea Valley, indicating that they have been formed at a stage at which ice had already receded from the Piancavallo Plateau. Finally, several large lateral moraine ridges are also preserved on the northern side of Monte Castelat, providing evidence of the evolution of a plateau glacier at this location, from which several glacial tongues extended towards the lower Cellina Valley.

4.1.3. The lacustrine succession in the Caltea Valley

In the upper part of the Caltea Valley, the homonymous river has strongly incised into the tectonically fractured bedrock and the overlying Quaternary deposits, offering insights into the composition of the former valley floor. Fuchs (1969) recognised the presence of laminated, silty sediments that crop out at two locations along a forest road on the right side of the valley, ca. 80 m above the present river level (12,52854°E; 46,12733°N; ca. 902 m a.s.l.; see Fig. 3). Inside a small ravine (section CAL-A), these sediments reach a thickness of around 8 m and are deposited on top of a unit of cemented, sandy gravels (Fig. 7a). The silt is characterised by a dark brown colour and fine, horizontal lamination, compatible with lacustrine deposition. Remarkable is that the sediments contain a large variety of plant macrofossils, ranging from needles and cones to pieces of bark and smaller twigs (Fig. 7b). Fuchs (1969) reports that these remains can largely be related to spruce (*Picea abies*) and larch (*Larix*) trees that were growing in the vicinity of the former lake basin. Most macrofossils are characterised by a distinct post-depositional flattening, with long axes aligned subparallel to the lamination plains, indicating that they were buried within the lake sediments during deposition. In the upper part of the section, the colour of the silt changes from dark brown to a lighter grey and organic macrofossils are notably absent. The silt is covered by a unit of well-sorted sandy gravels and ultimately capped by a thick layer of matrix-supported overconsolidated diamict containing edge-rounded and striated limestone clasts. A second outcrop, with a similar stratigraphy, was discovered at a forest road cut ca. 150 m up-valley from the ravine (section CAL-B, Fig. 7c). Here, the lacustrine deposits are less thick, and the sediments contain higher fractions of sand, potentially reflecting a more proximal sediment source. Plant remains, however, still occur frequently, with the largest macrofossil, a tree trunk, reaching a length of ca. 60 cm (Fig. 7d).

Table 1. Laboratory results for AMS radiocarbon measurements from macrofossils in the lacustrine section of the Caltea Valley.

	Section CAL-A						Section CAL-B			
Sample	**Material**	**^{14}C age (BP)**	**$F^{14}C$**	**$\delta^{13}C$ (‰)**		**Sample**	**Material**	**^{14}C age (BP)**	**$F^{14}C$**	**$\delta^{13}C$ (‰)**
CAL-A1	Wood (branch)	>46400*	<0.003	-24.1		CAL-B4	Wood (branch)	>54000*	<0.002	-20.7
CAL-A2	Wood (branch)	>49000*	<0.002	-22.4		CAL-B6	Wood (branch)	>49400*	<0.003	-23.4
CAL-A3	Wood (bark)	>52300*	<0.001	-25.6		CAL-B8	Wood (bark)	>51300*	<0.002	-27.6
CAL-A4	Wood (branch)	>50300*	<0.002	-24.2		CAL-B9	Wood (trunk)	>50300*	<0.002	-23.3
CAL-A5	Wood (twig)	>49200*	<0.002	-24.7						
CAL-A6	Wood (twig)	>45500*	<0.003	-22.8		*All ^{14}C ages are infinite				

Previously, the age of the lacustrine sediments was constrained by only a single radiocarbon date (29,350 ± 460 ^{14}C yr BP), presented by Fuchs (1969). This measurement was subsequently interpreted as a maximum age for the onset of glacier expansion in the southern Alps. For a better chronological resolution, a total of 10 new measurements was performed on macrofossil samples from both sections at different stratigraphic levels (see Fig. 7a). However, none of the samples yielded finite ^{14}C ages, with $F^{14}C$ being lower than 0.002 in most cases (Table 1). This indicates that the age of the sediments is either very close to or beyond the limit of the radiocarbon method, around 45,000 to 55,000 ^{14}C yr BP (Hajdas et al., 2021). These results are at odds with the age of Fuchs (1969), which we therefore advise to interpret with caution, keeping in mind that early radiocarbon chronologies have been revised in other parts of the Alps before (e.g., Spötl et al., 2013). In contrast, our new set of radiocarbon dates show that these sediments were deposited in a lake basin, well before the start of the climatic cooling during the global LGM. The abundance of plant macrofossils, especially large branches, and pieces of tree trunks, indicates deposition during an interglacial or interstadial period characterised by a mild climate that allowed the development of a boreal forest at this elevation. The transition to organic-free lacustrine and eventually fluvial sediments in the upper part of the section could then be evidence of a climatic cooling in the later part of this interstadial before the section was eventually overridden and partly eroded by the advance of the Caltea glacier. However, due to the non-finite nature of the radiocarbon dates, the exact chronology of this interstadial period remains unsolved at this point.

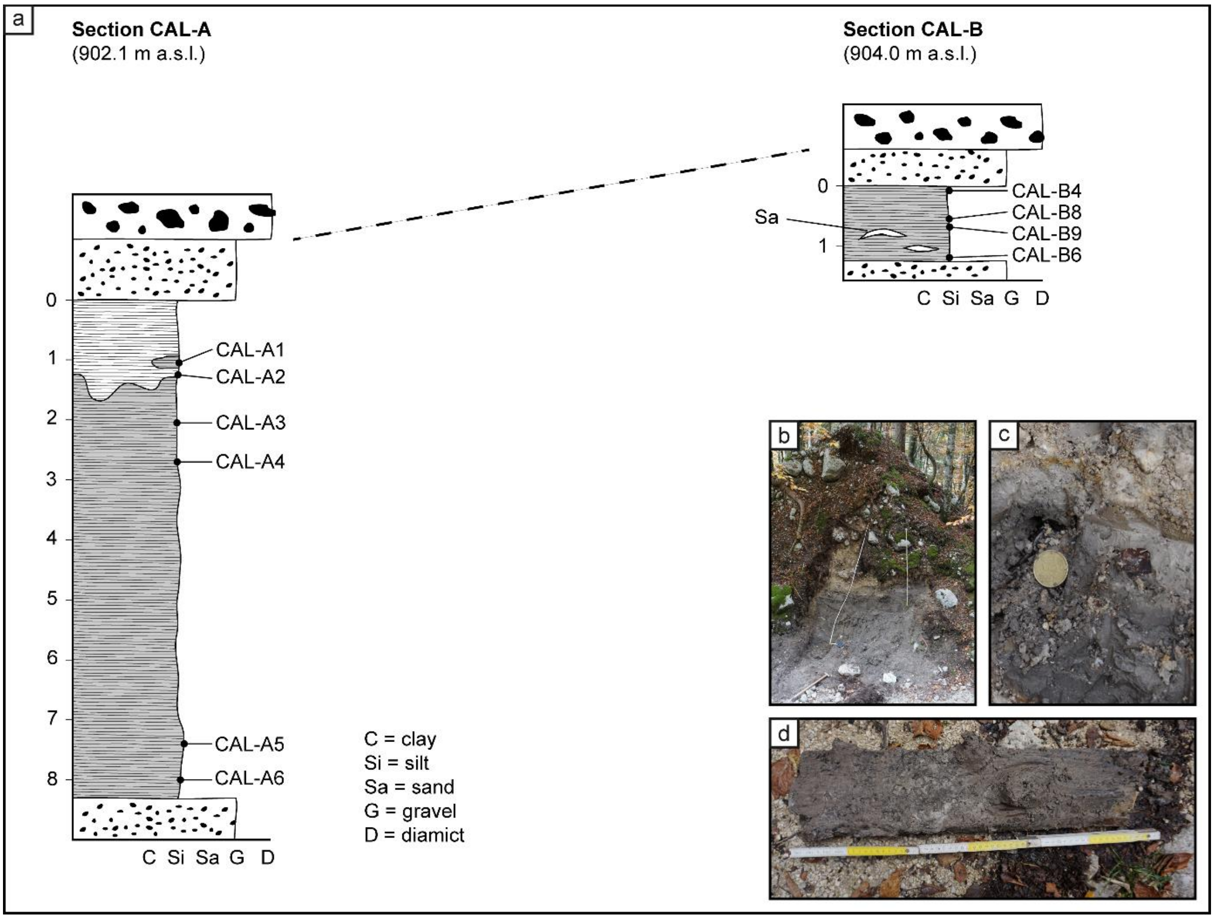

Fig. 7. The lacustrine sediments in the upper Caltea Valley. **a.** Sedimentary logs of the two sections CAL-A and CAL-B, with the locations of macrofossils that were sampled for radiocarbon dating. **b.** Photograph of section CAL-B, visible along a forest road cut. **c.** Close-up photograph of a plant macrofossil (sample CAL-A2), buried in the lacustrine sediments. Note the colour change from dark brown to light grey in this part of the section. **d.** The largest macrofossil found, a flattened tree trunk with a length of ca. 60 cm.

4.2. Palaeoglacier evolution and ELAs

4.2.1. The Monte Cavallo Group during the local LGM

The geomorphological evidence presented in the previous sections allowed to reconstruct the extent and evolution of palaeoglaciers in the MCG. The presence of two generations of moraine ridges in many valleys suggests at least two distinct cold phases that caused glaciers to advance or at least to stabilise. We regard the outer moraines to represent the local LGM as outside of these limits no glacial sediments and landforms were detected. The inner moraines relate to a post-LGM recessional phase at which glaciers had started to recede in the major valleys of the MCG. During the local LGM, glaciers in the MCG covered an elevation range of around 500 to 2050 m (Fig. 8). Several cirques represented the source areas for the Monte Cavallo Glacier, but ice also accumulated around Col Cornier (1767 m) and more importantly at Monte Castelat (1641 m), which hosted a separate plateau glacier (Castelat Glacier). From the accumulation areas, ice was flowing into the valleys on both sides of the main crestline. Towards the south and west, glaciers reached elevations between 800 m in the Stua, and 1100 m in the Seraie Valley. In the latter case, the glacier front came close to the upper limit of the Piave glacier, which has been reconstructed at 1040 m at Palughetto (Avigliano et al., 2000). Likely, however, the glaciers never fully merged, as opposed to those that occupied the valleys on the north-western flanks of Cimon del Cavallo (see Fig. 8). The longest glacier tongue of the Monte Cavallo Glacier flowed northwards through the Caltea Valley down to an elevation of around 500 m. Some authors have postulated that here it merged with a larger glacier from the Cellina Valley (Taramelli, 1875; Ehlers and Gibbard, 2004), however, several lines of evidence contradict this hypothesis: First, the morphology of the lower tract of the Cellina Valley appears to be dominantly shaped by fluvial erosion and does not indicate any glacial modification. Secondly, no exotic lithologies from the upper catchment of the Cellina, such as Triassic dolostones, were found in the tills of the lower Caltea Valley and on the northern side of the Castelat Plateau. Lastly, the Cellina catchment is generally characterised by relatively low elevations, and it is therefore unlikely that it provided large enough accumulation areas to sustain a prominent glacier tongue reaching into the lower tract of the valley. This is also reflected in a recent glacier modelling study (Seguinot et al., 2018) that suggest that the lower Cellina Valley remained ice-free during the entirety of the last glacial cycle.

In a few areas, such as the Stua Valley, minor uncertainties remain regarding the exact frontal position of glacial tongues, since moraine ridges have partially not been preserved in the valley bottoms. This is also the case for parts of the Castelat Glacier, especially in areas where ice was facing the steep slopes towards the Friulian Plain and preservation of landforms was therefore limited. Despite these uncertainties, there is a very good agreement between reconstructed ELAs for the Monte Cavallo and the Castelat glaciers. Applying the AABR method with a balance ratio of 1.56, ELAs were calculated at 1330 m and 1320 m. With an AAR of 0.58, reconstructed ELAs are somewhat higher, although the difference for the Cavallo Glacier is only around 40 m. These estimates also correlate with the MELM, that is at 1360 m in the Stua and Seraie valleys. Lower MELMs (ca. 1100 m) are recorded for lateral moraines on the northern side of the Castelat Plateau, which could relate to locally depressed ELAs due to lower ablation on the northerly facing slopes of the glacier.

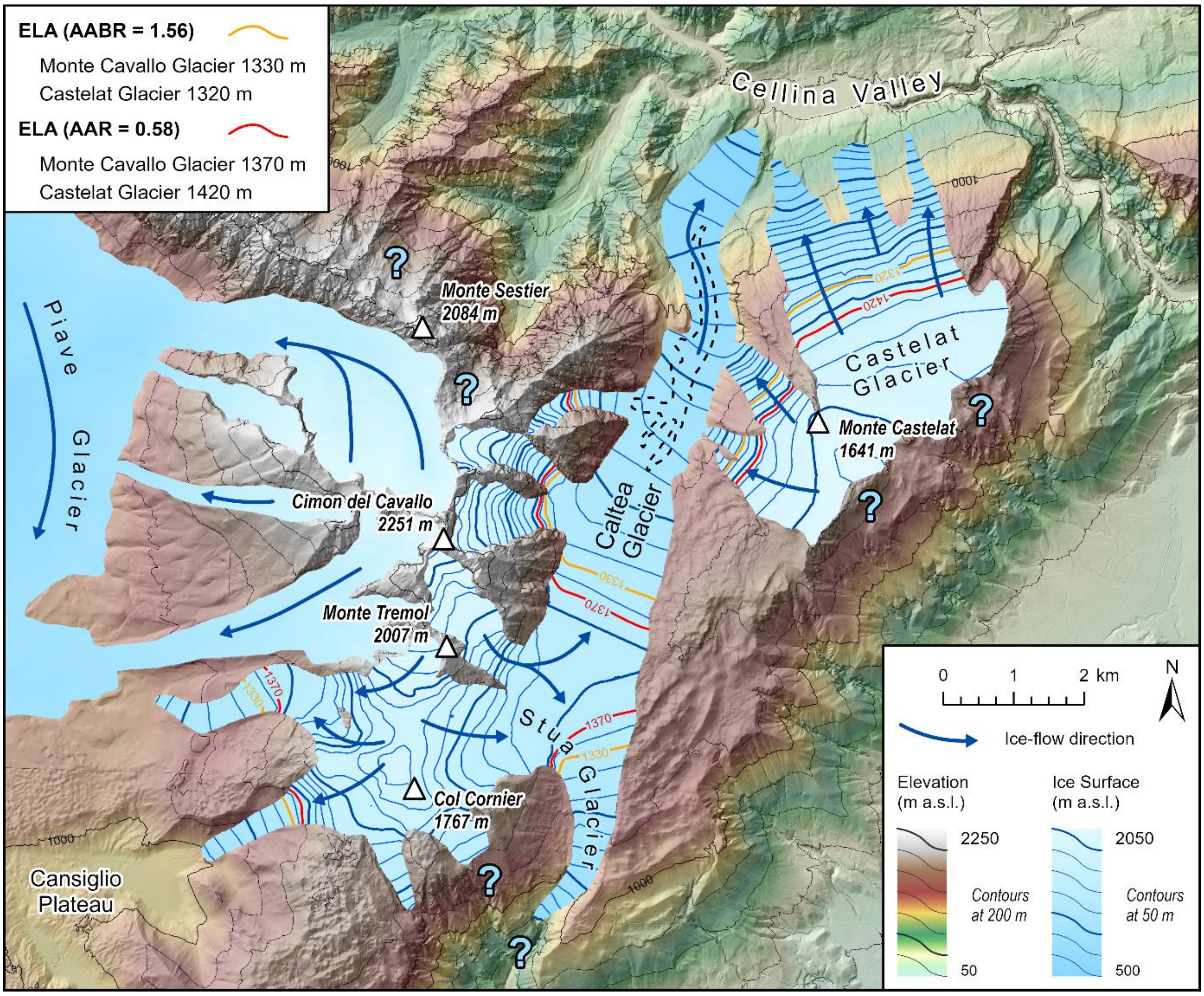

Fig. 8. Reconstructed glacier extent in the MCG during the local LGM. Blue question marks indicate areas of uncertain glacier extent. The black dashed line delimitates the area of the DEM that was modified before the final glacier modelling. ELAs were calculated both through the AABR and AAR-methods applying two different ratios each. Note that glaciers on the western side of the main divide were not reconstructed, as they probably merged with the large Piave Glacier that occupied the basin of Alpago. The upper limit of the Piave glacier was drawn according to Avigliano et al. (2000). Underlying elevation data: FVG-DEM (*eaglefvg.regione.fvg.it*). For additional toponyms and an overview regarding the geomorphological evidence see Fig. 3 and 4.

The presence of smaller, inner moraine ridges in the Caltea, Stua, and Bona valleys indicates that the early phase of glacier retreat after the local LGM was interrupted by at least one distinct phase of stagnancy or readvance. This advance was likely rather short-lived, as evident from the less pronounced morphologies of the moraines. It must have occurred relatively soon after the local LGM, since glaciers were still at an advanced position in many valleys. Nonetheless, this climatic change apparently had important effects on the configuration of the glacial system, especially in areas where ice was present near the ELA. The transverse moraine ridges at Pian delle More (cf. Fig. 5a, Fig. 6d) indicate that ice had quickly vanished from the northern part of the Piancavallo Plateau after the local LGM. The Caltea glacier was then only fed by tributaries from the Val Grande, Val Piccola and Caulana cirques and was no longer in connection with the outlets in the Stua, Bona and Seraie valleys. It is less clear how this climate change affected the glacier at Monte Castelat since no recessional moraines were found in the valleys on the northern side of the plateau. It is likely, however, that the Castelat glacier was affected to a stronger degree by this early phase of warming, due to its limited elevation range.

4.2.2. ELA reconstructions in other parts of the south-eastern Alps

The systematic reconstruction of palaeoglaciers in other parts of the south-eastern Alps resulted in a new set of ELAs that is reported in Table 2. For an AABR-value of 1.56, the recalculated ELAs for the valley glaciers in the Julian Prealps are between 1100 and 1160 m and show a very good agreement between individual catchments (Fig. 9a). A slightly higher ELA (1260 m) was determined for the glacier network at Monte Raut (Fig. 9b). Here, minor differences in the range of ca. 100 m can be noted between the three major tributaries, probably reflecting different degrees of shading and avalanche input in the relatively narrow lower valley tracts (Rettig et al., 2021). Similar observations can be made for the ice cap at Monte Grappa (Fig. 9c). While an ELA of 1450 m was determined for the entire system, lower ELAs (1360 m) characterise the outlet towards the North, whereas they are higher towards the West (1490 m) and the South (1510 m). Independent validation at this site is available from a smaller cirque glacier (Meatte Glacier) that is very well constrained by a set of frontal moraines and the ELA of which (1460 m) is essentially the same as for the larger ice cap in its vicinity (Baratto et al., 2003). The highest ELA was calculated for the Sette Comuni glacier at 1680 m (Fig. 9d). However, it must be noted that due to the notably larger size of this glacier with a prevalent southern exposure, potentially coupled to different dynamics, this latter estimate should be treated with greater caution. Applying different AABR- and AAR-values result in slightly varying ELA estimates (cf. Table 2), although for most sites the difference is only in the range of a few tens of meters. The largest discrepancy is observed for the Monte Raut glaciers, which is likely due to their rather unusual hypsometries which make especially ELA-estimates through the AAR-method less reliable (e.g., Benn and Lehmkuhl, 2000).

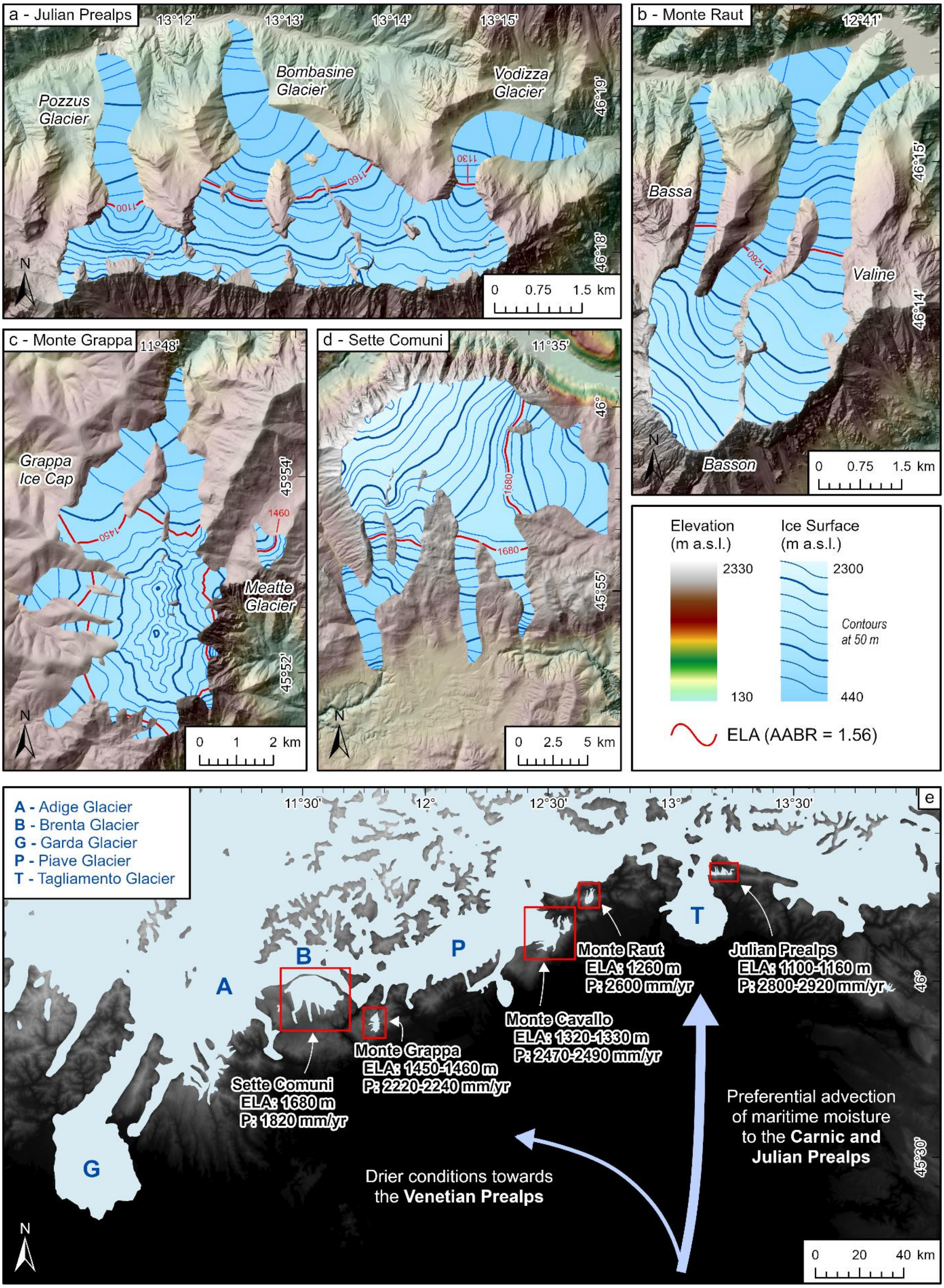

Fig. 9. Reconstructing palaeoglacier 3D geometries and ELAs in other parts of the south-eastern Alps. **a.** Valley glaciers on the northern slopes of the Chiampon-Cuel de Lanis ridge, Julian Prealps (after Monegato, 2012). **b.** The valley glacier system at Monte Raut (after Rettig et al., 2021). **c.** The Monte Grappa Ice Cap and the smaller Meatte Glacier (after Carraro and Sauro, 1979, Barrato et al., 2003). **d.** The Sette Comuni plateau glacier (after Barbieri et al., 2007). **e.** The south-eastern European Alps during the LGM with reconstructed ELAs (using an AABR ratio of 1.56) and palaeoprecipitation (P) for the glacier culmination during the early part of the LGM (ca. 25.5 to 23.5 ka). Glacier outlines updated from Ehlers and Gibbard (2004). Note the strong E-W gradient in ELAs and precipitation reflecting preferential advection of southerly derived moisture to the easternmost mountain ranges. Underlying elevation data: FVG-DEM (*eaglefvg.regione.fvg.it*) and EU-DEM v1.1. (*land.copernicus.eu*).

5. Discussion

5.1. Chronological control and timing of glacier advances

Chronological control is crucial to derive palaeoclimatic information from moraine records but so far no numerical datings have been reported from smaller glaciers in the south-eastern Alps. It remains therefore to be discussed if (a) the investigated moraines in the MCG are time-consistent to moraines in other areas of the south-eastern Alps and (b) if they correspond to the maxima of larger outlet glaciers that have been dated to the period of the global LGM. The attempt to better constrain the local LGM in the MCG through dating the lacustrine section in the Caltea Valley was not successful, as from the infinite nature of the radiocarbon dates an advance during MIS 3 or earlier cannot be ruled out with certainty. In the other pre-Alpine valleys, glacial sediments rarely contain datable organic material, contrary to lowland settings, where the radiocarbon method has been successfully applied to constrain LGM glacier advances in several instances (e.g., Jorda et al., 2000; Monegato et al., 2007; Ravazzi et al., 2012; Monegato et al., 2017). Additionally, limestone boulders on moraine ridges in the south-eastern Alps have been likely experienced substantial dissolution since the LGM, as demonstrated by the typical karstic landscape of this region, introducing notable uncertainties into a potential application of cosmogenic exposure dating (Levenson et al., 2017; Žebre et al., 2019).

Table 2. Characteristics of LGM palaeoglaciers in the south-eastern Alps, including ELAs calculated through the AABR- and AAR-methods. Key for glacier type: 1=single valley glacier, 2=valley glacier system, 3=plateau glacier, 4=ice cap, 5=cirque glacier. Note increasing ELAs going from East to West. Calculation of T_{Melt} was based on the chironomid record by Samartin et al. (2016) and extrapolated to the respective glacier ELAs using a standard altitudinal lapse rate of 6.5°C km^{-1}. Precipitation was estimated using the approach described in Ohmura and Boettcher (2018). Temperature and precipitation values correspond to an early regional LGM (25.5 to 23.5 ka) and in brackets to a late regional LGM (23 to 21 ka) advance. Modern (1971-2008) precipitation was extracted from the gridded dataset of Isotta et al. (2014) and averaged across the reconstructed glacier areas.

	Glacier name	Type	Elevation	Surface	ELA (AABR)		ELA (AAR)		T_{Melt} (ELA)	P (LGM)	P (1971-2008)
			(m a.s.l.)	(km^2)	1.29	1.56	0.58	0.67	(°C)	(mm/yr)	(mm/yr)
EAST	Vodizza Glacier	1	640-1580	1.78	1160	**1130**	**1150**	1010	7.0 (5.9) ± 1.6	2860 (2530) ± 750	2380 ± 410
	Bombasine Glacier	1	498-1621	4.16	1180	**1160**	**1210**	1130	6.8 (5.7) ± 1.6	2800 (2470) ± 750	2380 ± 410
	Pozzus Glacier	1	598-1743	1.67	1120	**1100**	**1110**	1000	7.2 (6.1) ± 1.6	2920 (2590) ± 750	2260 ± 390
	Monte Raut Glacier	2	439-2063	7.02	1300	**1260**	**1380**	1200	6.2 (5.1) ± 1.6	2600 (2280) ± 750	2230 ± 500
	Bassa tributary		538-1769	0.82	1200	**1170**	**1170**	1080			
	Basson tributary		439-2063	3.26	1310	**1270**	**1400**	1210			
	Valine tributary		445-1850	2.93	1310	**1290**	**1420**	1260			
	Cavallo Glacier	2	504-2056	24.37	1350	**1330**	**1370**	1370	5.7 (4.6) ± 1.6	2470 (2150) ± 750	2030 ± 410
	Castelat Glacier	3	582-1656	12.37	1340	**1320**	**1430**	1430	5.8 (4.7) ± 1.6	2490 (2170) ± 750	2170 ± 510
	Grappa Ice Cap	4	895-1807	12.32	1460	**1450**	**1460**	1460	4.9 (3.8) ± 1.6	2240(1930) ± 750	1610 ± 300
	N-Outlet		895-1803	5.45	1370	**1360**	**1370**	1340			
	W-Outlet		1145-1807	2.13	1510	**1490**	**1510**	1450			
	S-Outlet		1270-1802	2.27	1520	**1510**	**1520**	1500			
	Meatte Glacier	5	1318-1619	0.28	1460	**1460**	**1470**	1450	4.9 (3.8) ± 1.6	2220 (1910) ± 750	1600 ± 260
WEST	Sette Comuni Glacier	3	898-2305	98.33	1710	**1680**	**1690**	1610	3.4 (2.3) ± 1.6	1820 (1530) ± 740	1450 ± 270

Therefore, we primarily rely on geomorphological and stratigraphical evidence to relate moraine ridges between different sites and to those deposits that have chronologically been constrained. The absence of cementation and deep weathering in all the observed glacial sediments in the MCG allows to exclude that they pertain to a major glaciation before the global LGM (e.g., MIS 6 one or older). Regionally, soils on glacial deposits and moraine ridges from such previous glaciations are luvosoils, characterised by well-developed Bt-horizons (cf. Provincia di Treviso and ARPAV, 2008), which were not observed on any glacial deposits in the MCG. Glacier advances during MIS 3 or MIS 4 are also unlikely. Gribenski et al. (2021) recently reported new luminescence data that support MIS 4 and late MIS 3 advances along the western side of the Alps. However, climatic conditions at the opposite side of the Alpine arc, around 500 km West of the MCG, were likely very different from those along the south-eastern Alpine fringe and no MIS 3 or MIS 4 advances have been reported from amphitheatres in the southern central (Braakhekke et al., 2020; Kamleitner et al., 2022) and south-eastern (Monegato et al., 2007; 2017) part of the Alps.

Additional chronological evidence comes from alluvial fans throughout the Venetian and Friulian Plain, where maximum aggradation was dated to the period of the global LGM (26 to 21 cal ka BP, Fontana et al., 2014) throughout the Tagliamento (Monegato et al., 2007), Brenta (Rossato and Mozzi, 2016), Piave (Carton et al., 2009) and Cellina Fans (Avigliano et al., 2002). In the Brenta fan, for example, the maximum aggradation has been constrained between 26.7 and 23.8 cal ka BP (Rossato and Mozzi, 2016), corresponding very closely to glacier maxima in the Garda and Tagliamento amphitheatres. This synchronous response throughout the alluvial fans is despite the fact that they are connected to hydrological basins of different sizes and elevations. The Cellina Fan, for example has been largely fed by smaller glacial systems, including those glaciers of the MCG. The Tagliamento fan, on the other hand, is related to a large outlet glacier that received considerable input from more internal valleys of the Alps.

In the MCG, we have recognised a distinct two-fold LGM advance, where large, external moraines represent the maximum glacier extent and smaller, internal moraines can be related to an early stage of ice recession (Fig. 10a). At a closer look, similar patterns can be found in other areas of the south-eastern Alps. In the Julian Prealps, for example, two generations of moraine ridges are clearly visible both in the Pozzus (Fig. 10b) and in the Vodizza Valleys (Fig. 10c). Here, the external moraine ridges are equally large and prominent (ca. 20-30 m), while the recessional ridges are characterised by more subtle morphologies. Also in the Busetto Valley, two moraine crestlines delineate the lateral extent of the western outlet of the Monte Grappa Ice Cap, although the morphological differences are less pronounced here. The common geomorphological pattern indicates that glacier advances in the south-eastern Alps were likely synchronous among different mountain ranges, and that the glaciers responded to a regional climatic forcing rather than to catchment-specific factors. It is likely that this two-fold pattern corresponds to the two periods of glacier culmination that were reconstructed in the Garda and Tagliamento amphitheatres (See Fig. 2, Monegato et al., 2007; 2017). We therefore propose that the outer moraine ridges (local LGM) in the MCG and other mountain ranges in the south-eastern Alps correspond to an early LGM (25.5 to 23.5 ka) advance while the inner moraines relate to a recessional phase during the latter part of the LGM (23 to 21 ka).

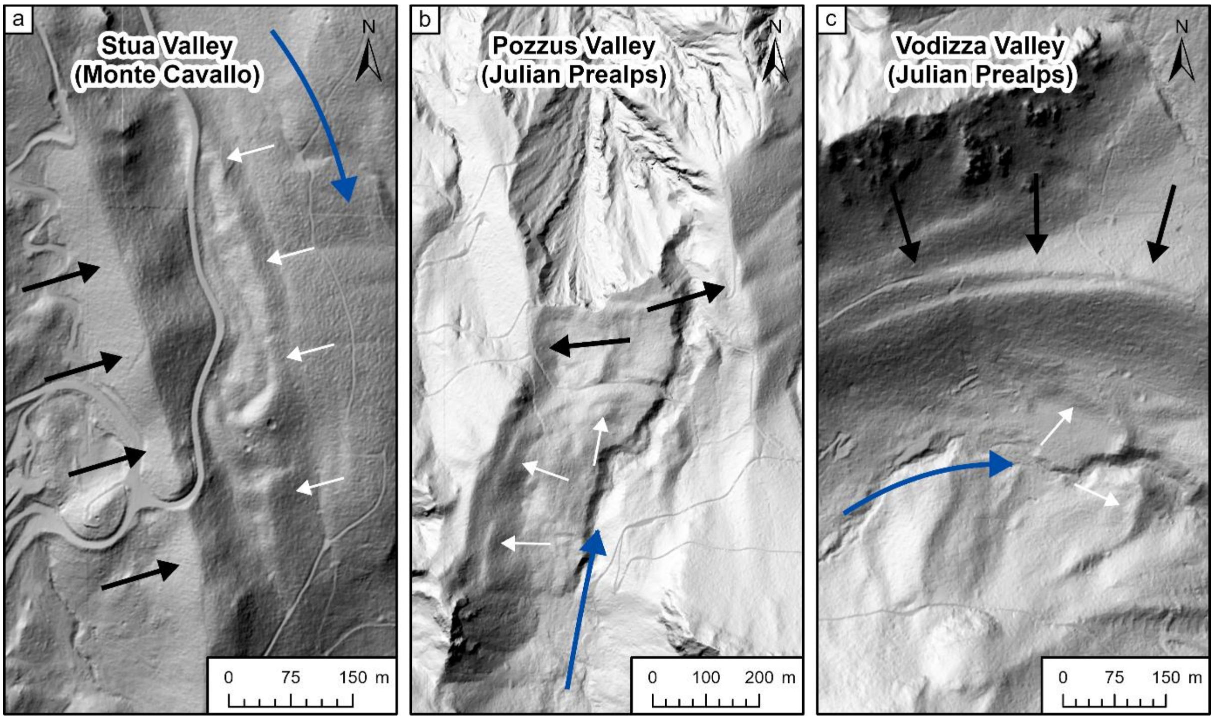

Fig. 10. A common chronological pattern for LGM glacier advances in the south-eastern Alps is suggested by the position and morphology of moraine ridges in the pre-Alpine valleys. Large, outer moraines are marked with thick, black arrows while smaller inner moraines with thinner, white arrows. Ice-flow directions are indicated by a blue arrow. **a.** The upper Stua Valley in the MCG. **b.** The Pozzus Valley in the Julian Prealps. **c.** The Vodizza Valley in the Julian Prealps. Underlying elevation data: FVG-DEM (*eaglefvg.regione.fvg.it*).

5.2. The ELA in the south-eastern Alps during the LGM

Our new ELA estimates are in general agreement with those that have been previously reported for the south-eastern Alps, ranging from around 1100 to 1700 m (Penck and Brückner, 1909; Pasa, 1940; Fuchs, 1970; Mattana, 1974; Carraro and Sauro, 1979; Baratto et al., 2003; Monegato, 2012; Rettig et al., 2021). In fact, in most cases remodelled ELAs agree well with those that were derived through traditional approaches. In the MCG, for example, our numerically reconstructed ELAs of 1330 and 1320 m are only marginally different from that calculated by Fuchs (1970) at 1350 m. Slightly larger differences (in the order of ca. 50 m) can be noted for the recalculated ELAs of the glaciers at Monte Grappa and in the Julian Prealps.

From the reconstructed values it is apparent that an ELA gradient existed across the southern fringe of the Alps during the local LGM, with ELAs being lowest in the easternmost part of the Julian and Carnic Prealps and gradually rising towards the Venetian Prealps in the West (Fig. 9e). Over a horizontal distance of around 150 km, calculated ELAs vary by more than 500 m, pointing to strong differences within climatic boundary conditions that allowed glaciers in the eastern mountain ranges to descend to lower elevations. This ELA-gradient may partly overestimate the true climatic gradient owing to the influence of topographic factors and palaeoglacier aspect. In the Julian and Carnic Prealps, valley glaciers were oftentimes confined to narrow, north-facing valleys with avalanche input potentially lowering the climatic ELA (Coleman et al., 2009; Chandler and Lukas, 2017). The glaciers towards the West, on the other hand, are characterised by a gentler topography and a dominantly southerly exposure. However, it is unlikely that these factors can fully explain the observed trend in ELAs, as site-specific, topographically controlled lowering of the climatic ELA is usually in the range of 50-150 m for Alpine glaciers (Žebre et al., 2021). Additionally, our investigation shows that glaciers of different sizes and elevation ranges yield similar ELAs (e.g., Cavallo vs. Castelat Glacier, Monte Grappa vs. Monte Meatte glacier). Lastly, the reconstructed ELA gradient accurately reflects modern precipitation gradients in the region (cf. Fig. 1b), and it is therefore not unreasonable to assume that such gradients also persisted along the southern fringe of the Alps during the LGM.

5.3. LGM precipitation patterns in the south-eastern Alps

In section 5.2., we have demonstrated that an ELA gradient existed along the south-eastern fringe of the Alps during the local LGM. Glacier ELAs are influenced both by temperature and precipitation, but since large temperature changes over small spatial scales are unlikely, the lower ELAs in the eastern parts of the Carnic and Julian Prealps probably reflect differences in the advection of precipitation at these sites. Without quantitative precipitation estimates, however, it remains unclear if this is compatible with modern climatic settings or if higher or lower amounts of precipitation are needed to explain the observed glacier ELAs. As we have demonstrated in section 5.1., the ELAs likely relate to the period of the early regional LGM advance between 25.5 and 23.5 ka. For this scenario, reconstructed precipitation is in the range between 1820 ± 750 mm/yr at the Sette Comuni Glacier and up to 2920 ± 750 mm/yr in the Julian Prealps (Table 2). For the scenario of a late LGM advance (23 to 21 ka), precipitation is somewhat lower and ranges from 1530 ± 750 mm/yr to 2590 ± 750 mm/yr. Despite the uncertainties involved in the calculations, both the spatial pattern and reconstructed precipitation totals are largely compatible with what is measured at modern weather stations in the region (Fig. 11). This means that the regional LGM precipitation regime in the south-eastern Alps was likely similar to today, despite fundamental changes in the overall climatic setting and the palaeogeography of the Adriatic Sea. It also clearly demonstrates that high precipitation in the easternmost southern Alps was necessary to allow larger glacial systems to develop, despite their relatively low-elevated catchments (cf. Monegato et al., 2007).

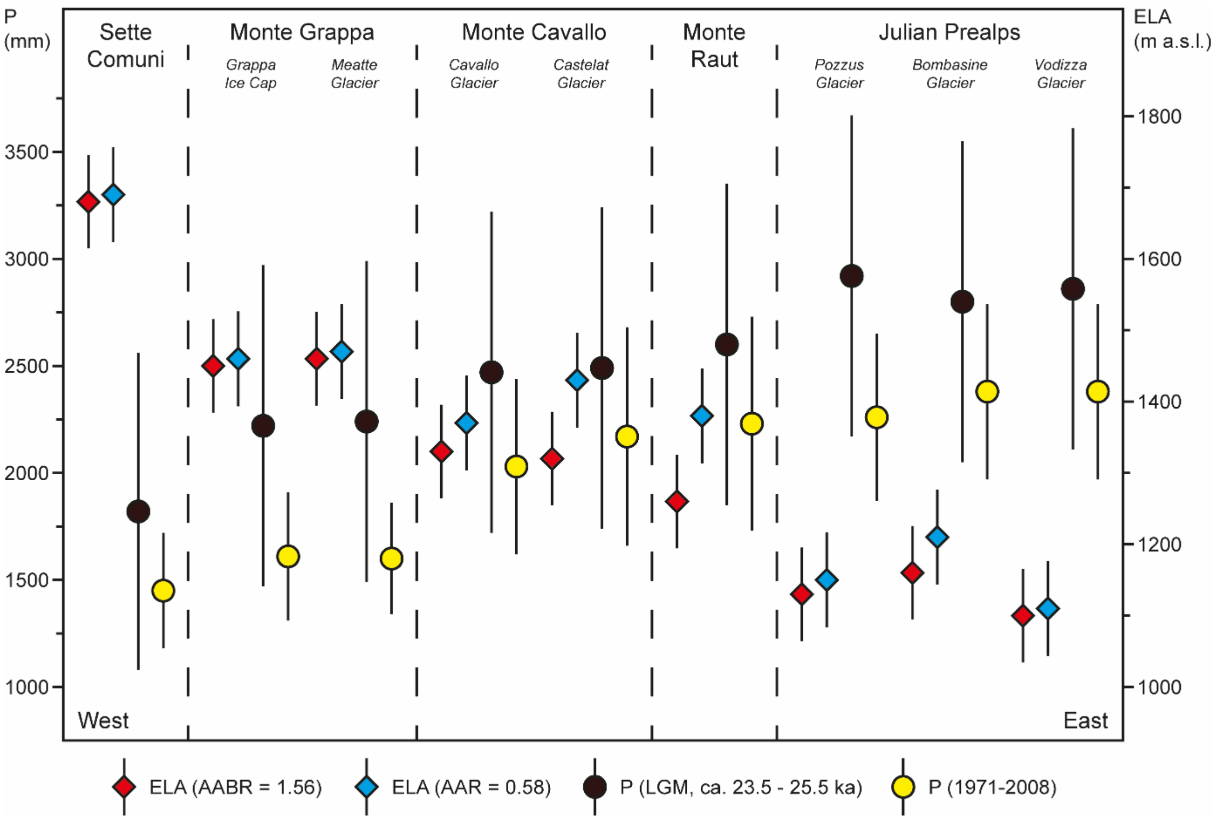

Fig. 11. Boxplot visualising reconstructed ELAs and palaeoprecipitation for the study sites in the south-eastern Alps. The gradient within ELAs and precipitation is clearly visible moving from West to East. Uncertainties in reconstructed ELAs are the median differences between calculated ELAs, using the median global AABR and AAR ratios, and measured ELAs from mass-balance time series (Oien et al. ,2022). Reconstructed LGM precipitation refers to the period between ca. 25.5 and 23.5 ka. Precipitation data for the period 1971-2008 was derived from the gridded dataset of Isotta et al. (2014) and averaged across the area of the reconstructed glaciers.

The high LGM precipitation in the south-eastern Alps merits further discussion, especially since for other sectors of the Alps, such as the Maritime Alps (Ribolini et al., 2022) or the Northern Alps (Becker et al., 2016), a reduction in LGM precipitation has been reconstructed both through palaeoclimate proxies and via glacier modelling. On the one hand our calculations may slightly over-estimate precipitation in some instances due to topoclimatic factors lowering the effective glacier ELA from the environmental one (Žebre et al., 2021; cf. section 5.2.). Also, the reported July temperatures at Lago della Costa cannot be considered representative for the entirety of the south-eastern Alps owing to microclimatic conditions in the refugia of the Euganean Hills (Samartin et al., 2016). However, new pollen-based temperature reconstructions from Lake Fimon (Pini et al., 2022) equally indicate July temperatures around 13.6°C for most of the global LGM, an average of the values used in our calculations. Conclusively, our data shows that the mountain ranges along the south-eastern Alpine fringe have received continuous moisture supply during the global LGM from the Adriatic Sea. This was likely possible due to a southward shift of the North Atlantic jet stream that increased the advection of southerly moisture sources to the Alps in general (e.g., Florineth and Schlüchter, 2000). This climatic shift affected the southern Alpine fringe stronger than any other sector of the Alps as it is the first part of the Alps intersecting humid air masses coming from this cardinal direction. If the precipitation predominantly occurred during the winter months (cf. Spötl et al., 2021) it would have provided enough accumulation to sustain glaciers also in these lower parts of the Alps.

In recent years, the application of numerical models in palaeoclimate research has gained increased attention, with studies aiming to reconstruct environmental ELAs at an Alpine scale. Our results allow to test and validate the performance of such models against field-based data within a specific sector of the Alps. Del Gobbo et al. (2022), for instance, have reconstructed ELAs throughout the Alps using a regional climate model and their results show an overall good agreement with those determined from geomorphological evidence. In particular, the ELA depression in the Eastern Carnic and Julian Prealps is sufficiently represented in this model. Other approaches (Višnjević et al., 2020) and general circulation models (Kuhlemann et al., 2008) show greater discrepancies and are particularly unable to reflect variations of the ELA over smaller spatial scales. This highlights the importance of local climatic conditions for the evolution of Alpine glaciers in general, and during the LGM in particular and therefore more data will be needed from other parts of the Alps to test and improve such models. In the western Alps, glacier-based ELA reconstructions have been reported from the Dorea Baltea catchment (Forno et al., 2010) and the Maritime Alps (Federici et al., 2012). These ELAs are higher, indicating a drier and/or warmer climate during the LGM. Data is specifically sparse in the central Alps, where palaeoclimate models have reconstructed high LGM precipitation (Del Gobbo et al., 2022). Here, the extent and chronology of the Ticino-Toce system have recently been presented (Kamleitner et al., 2022), but ELA estimates from smaller glaciers are absent for this part of the Alps. This highlights the need for further research in other Alpine regions to construct a more complete picture of LGM precipitation and its influence on the evolution of Alpine glaciers.

6. Conclusions

In this study we have presented new data concerning the evolution of palaeoglaciers in the Monte Cavallo Group (Venetian Prealps, NE-Italy) during the local Last Glacial Maximum (LGM). We have used glacial geomorphological mapping in combination with semi-automated GIS tools to reconstruct palaeoglacier geometries and their Equilibrium Line Altitudes (ELA), which have enabled us to gain better insights into the LGM palaeoclimate of the south-eastern Alps. The following points can be concluded from our study:

- During the local LGM, the Monte Cavallo Group hosted a glacial system that was fully detached from larger outlet glaciers of the Alpine ice sheet and therefore likely responded very dynamically to climatic changes.
- Remodelling of palaeoglaciers in other parts of the south-eastern Alps shows that ELAs during the regional LGM (ca. 25.5 to 23.5 ka) were in the range of ca. 1100 to almost 1700 m. A strong ELA gradient existed along the Alpine fringe, with a lowering from West to East. Precipitation concentrated in the Julian and eastern Carnic Prealps, while the Venetian Prealps received a more limited moisture supply.
- Both patterns and calculated annual precipitations are largely compatible with what is observed in the modern-day climate where moisture supply from the Adriatic Sea leads to long lasting orographic precipitation.

- The lacustrine section in the Caltea Valley, which has been widely used as a chronological constrain for the onset of the LGM in the south-eastern Alps, dates back to an older interglacial or interstadial period, beyond the limit of the radiocarbon method.

Acknowledgements

The authors would like to thank Francesco Ferrarese for providing spatial data that enabled the reconstruction of the Monte Grappa Glacier, and Renato R. Colucci for assisting with field sampling. This work was supported by the Royal Society [grant number: IEC\R2\202123].

Reference List

Allard, J.L., Hughes, P.D., Woodward, J.C., Fink, D., Simon, K., Wilcken, K.M., 2020. Late Pleistocene glaciers in Greece: A new ^{36}Cl chronology. Quat. Sci. Rev. 245, 106528. https://doi.org/10.1016/j.quascirev.2020.106528.

Avigliano, R., Anastasio, G.D., Improta, S., Peresani, M., Ravazzi, C., 2000. A new late glacial to early Holocene palaeobotanical and archaeological record in the Eastern Pre-Alps: the Palughetto basin (Cansiglio Plateau, Italy). J. Quat. Sci. 15, 789-803. https://doi.org/10.1002/1099-1417(200012)15:8<789::AID-JQS556>3.0.CO;2-E.

Avigliano, R., Calderoni, G., Monegato, G., Mozzi, P., 2002. The late Pleistocene-Holocene evolution of the Cellina and Meduna alluvial fans (Friuli, NE Italy). Mem. Soc. Geol. It. 57, 133-139.

Baratto, A., Ferrarese, F., Meneghel, M., Sauro U., 2003. La ricostruzione della glaciazione Wurmiana nel Gruppo del Monte Grappa (Prealpi Venete), in: Biancotti, A., Motta, M. (Eds.), Risposta dei processi geomorfologici alle variazioni ambientali. Brigati G., Genova, pp. 67-77.

Barbieri, G., Grandesso, P., 2007. Geological map and explanatory notes of the Geological Map of Italy at the scale 1:50.000: Sheet 082 “Asiago”. APAT, Dipartimento Difesa del Suolo-Servizio Geologico d’Italia, Rome.

Baroni, C., Guidobaldi, G., Salvatore, M.C., Christl, M., Ivy-Ochs, S., 2018. Last glacial maximum glaciers in the Northern Apennines reflect primarily the influence of southerly storm-tracks in the western Mediterranean. Quat. Sci. Rev. 197, 352-367. https://doi.org/10.1016/j.quascirev.2018.07.003.

Barr, I.D., Spagnolo, M., 2015. Glacial cirques as palaeoenvironmental indicators: Their potential and limitations. Earth Sci. Rev. 151, 48-78. https://doi.org/10.1016/j.earscirev.2015.10.004.

Becker, P., Seguinot, J., Jouvet, G., Funk, M., 2016. Last Glacial Maximum precipitation pattern in the Alps inferred from glacier modelling. Geogr. Helv. 71, 173-187. https://doi.org/10.5194/gh-71-173-2016.

Benn, D.I., Ballantyne, C.K., 2005. Palaeoclimatic reconstruction from Loch Lomond Readvance glaciers in the West Drumochter Hills, Scotland. J. Quat. Sci. 20, 577-592. https://doi.org/10.1002/jqs.925.

Benn, D.I., Lehmkuhl, F., 2000. Mass balance and equilibrium-line altitudes of glaciers in high-mountain environments. Quat. Int. 65/66, 15-29. https://doi.org/10.1016/S1040-6182(99)00034-8.

Benn, D.I., Hulton, N.R.J., 2010. An Excel™ spreadsheet program for reconstructing the surface profile of former mountain glaciers and ice caps. Comput. Geosci. 36, 605-610. https://doi.org/10.1016/j.cageo.2009.09.016.

Bernsteiner, H., Götz, J., Salcher, B.C., Lang, A., 2021. From deglaciation to postglacial filling: post-LGM evolution of an isolated glacier system at the northern fringe of the Eastern Alps (Austria). Geogr. Ann. Ser. A Phys. Geogr. 103, 305-322. https://doi.org/10.1080/04353676.2021.1933958.

Bondesan, A., Calderoni, G., Mozzi, P., 2002. L'assetto geomorfologico della pianura veneta centro-orientale: stato delle conoscenze e nuovi dati, in: Varotto, M., Zunica, M. (Eds.), Scritti in ricordo di Giovanna Brunetta. Università degli Studi di Padova, Dipartimento di Geografia, Padova, pp. 19-38.

Braakhekke, J., Ivy-Ochs, S., Monegato, G., Gianotti, F., Martin, S., Casale, S., Christl, M., 2020. Timing and flow pattern of the Orta Glacier (European Alps) during the Last Glacial Maximum. Boreas 49, 315-332. https://doi.org/10.1111/bor.12427.

Burke, R., Birkeland, P., 1979. Reevaluation of Multiparameter Relative Dating Techniques and their Application to the Glacial Sequence Along the Eastern Escarpment of the Sierra Nevada, California. Quat. Res., 11, 21-51. https://doi.org/10.1016/0033-5894(79)90068-1.

Cancian, G., Ghetti, S., Semenza, E., 1985. Aspetti geologici dell'Altipiano del Cansiglio. Lav. Soc. Ven. Sci. Nat., Suppl. 10, 79-90.

Carraro, F., Sauro, U., 1979. Il Glacialismo "locale" Wurmiano del Massiccio del Grappa (Provincie di Treviso e di Vicenza). Geogr. Fis. Din. Quat. 2, 6-16.

Carton, A., Bondesan, A., Fontana, A., Meneghel, M., Miola, A., Mozzi, P., Primon, S., Surian, N., 2009. Geomorphological evolution and sediment transfer in the Piave River system (northeastern Italy) since the Last Glacial Maximum. Gemorph. Relief Process. Environ. 15, 155-174. https://doi.org/10.4000/geomorphologie.7639.

Carulli, G.B., Podda, F., Venturini, C., Zanferrari, A., Cucchi, F., Monegato, G., Nicolich, R., Paiero, G., Piano, C., Slejko, D., Tunis, G., Zanolla, C., 2006. Carta Geologica del Friuli Venezia Giulia (Scala 1:150.000). Edizioni S.EL.CA., Firenze.

Castiglioni, B., 1940. L'Italia nell'età quaternaria. Carta alla scala 1:200000. Atlante Fisico-Economico d'Italia, TCI, Milano.

Castiglioni, G.B., 1964. Forme del Carsismo superficiale dell'Altipiano del Cansiglio. Atti Ist. Veneziano Sci. Lett. Arti 122, 327-344.

Chandler, B.M., Lukas, S., 2017. Reconstruction of Loch Lomond Stadial (Younger Dryas) glaciers on Ben More Coigach, north-west Scotland, and implications for reconstructing palaeoclimate using small ice masses. J. Quat. Sci. 32, 475-492. https://doi.org/10.1002/jqs.2941.

Chandler, B.M.P., Lovell, H., Boston, C.M., Lukas, S., Barr, I.D., Benediktsson, Í.Ö., Benn, D.I., Clark, C.D., Darvill, C.M., Evans, D.J.A., Ewertowski, M.W., Loibl, D., Margold, M., Otto, J., Roberts, D.H., Stokes, C.R., Storrar, R.D., Stroeven, A.P., 2018. Glacial geomorphological mapping: A review of approaches and frameworks for best practice. Earth Sci. Rev. 185, 806-846. https://doi.org/10.1016/j.earscirev.2018.07.015.

Chandler, B.M., Boston, C.M., Lukas, S., 2019. A spatially-restricted Younger Dryas plateau icefield in the Gaick, Scotland: Reconstruction and palaeoclimatic implications. Quat. Sci. Rev., 211, 107-135. https://doi.org/10.1016/j.quascirev.2019.03.019.

Clark, P.U., Dyke, A.S., Shakun, J.D., Carlson, A.E., Clark, J., Wohlfarth, B., Mitrovica, J.X., Hostetler, S.W., McCabe, A.M., 2009. The last glacial maximum. Science 325, 710-714. https://doi.org/10.1126/science.1172873.

Coleman, C.G., Carr, S.J., Parker, A.G., 2009. Modelling topoclimatic controls on palaeoglaciers: implications for inferring palaeoclimate from geomorphic evidence. Quat. Sci. Rev. 28, 249-259. https://doi.org/10.1016/j.quascirev.2008.10.016.

Colman, S., Pierce, K., 1986. Glacial Sequence Near McCall, Idaho: Weathering Rinds, Soil Development, Morphology, and Other Relative-Age Criteria. Quat. Res. 25, 25-42. https://doi.org/10.1016/0033-5894(86)90041-4.

Colucci, R.R., Guglielmin, M., 2015. Precipitation-temperature changes and evolution of a small glacier in the southeastern European Alps during the last 90 years. Int. J. Climatol. 35, 2783-2797. https://doi.org/10.1002/joc.4172.

Colucci, R.R., Žebre, M., Torma, C.Z., Glasser, N.F., Maset, E., Del Gobbo, C., Pillon, S., 2021. Recent Increases in Winter Snowfall Provide Resilience to Very Small Glaciers in the Julian Alps, Europe. Atmosphere 12, 263. https://doi.org/10.3390/atmos12020263.

Crespi, A., Brunetti, M., Lentini, G., Maugeri, M., 2018. 1961-1990 high-resolution monthly precipitation climatologies for Italy. Int. J. Climatol. 38, 878-895. https://doi.org/10.1002/joc.5217.

Del Gobbo, C., Colucci, R.R., Monegato, G., Žebre, M., Giorgi, F., 2022. Atmosphere-cryosphere interactions at 21 ka BP in the European Alps. Clim. Past, preprint. https://doi.org/10.5194/cp-2022-43.

Ehlers, J., Gibbard, P.L., 2004. Quaternary glaciations-extent and chronology: part I: Europe. Elsevier, Amsterdam.

Evans, D.J.A., Phillips, E.R., Hiemstra, J.F., Auton, C.A., 2006. Subglacial till: formation, sedimentary characteristics and classification. Earth Sci. Rev. 78, 115-176. https://doi.org/10.1016/j.earscirev.2006.04.001.

Evans, D.J.A., Benn, D.I., 2021. Facies description and the logging of sedimentary exposures, in: Evans, D.J.A., Benn, D.I. (Eds.), A practical guide to the study of glacial sediments. Arnold, London, pp. 11-51.

Federici, P.R., Granger, D.E., Ribolini, A., Spagnolo, M., Pappalardo, M., Cyr, A.J., 2012. Last Glacial Maximum and the Gschnitz stadial in the Maritime Alps according to 10Be cosmogenic dating. Boreas 41, 277-291. http://doi.org/10.1111/j.1502-3885.2011.00233.x.

Filippini, M., Squarzoni, G., De Waele, J., Fiorucci, A., Vigna, B., Grillo, B., Riva, A., Rossetti, S., Zini, L., Casagrande, G., Stumpp, C., Gargini, A., 2018. Differentiated spring behavior under changing hydrological conditions in an alpine karst aquifer. J. Hydrol. 556, 572-584. https://doi.org/10.1016/j.jhydrol.2017.11.040.

Florineth, D., Schlüchter, C., 2000. Alpine Evidence for Atmospheric Circulation Patterns in Europe during the Last Glacial Maximum. Quat. Res. 54, 295-308. https://doi.org/10.1006/qres.2000.2169.

Fontana, A., Mozzi, P., Marchetti, M., 2014. Alluvial fans and megafans along the southern side of the Alps. Sediment. Geol. 301, 150-171. https://doi.org/10.1016/j.sedgeo.2013.09.003.

Forno, M.G., Gianotti, F., Racca, G., 2010. Significato paleoclimatico dei rapporti tra il glacialismo principale e quello tributario nella bassa Valle della Dora Baltea. Alp. Mediterr. Quat. 23, 105-124.

Fuchs, F., 1969. Eine erste 14C-Datierung für das Paudorf-Interstadial am Alpensüdrand: Fossiles Holz aus dem Val Caltea in der Monte Cavallo-Gruppe, Venezianische Voralpen (Italien). Eiszeitalter Ggw. 20, 68-71. https://doi.org/10.3285/eg.20.1.05.

Fuchs, F., 1970. Studien zur Karst-und Glazialmorphologie in der Monte Cavallo-Gruppe/Venezianische Voralpen (Italien). Frankf. Geogr. Hefte 47.

Furbish, D.J., Andrews, J.T., 1984. The use of hypsometry to indicate long-term stability and response of valley glaciers to changes in mass transfer. J. Glaciol. 30, 199-211. https://doi.org/10.3189/S0022143000005931.

Gianotti, F., Forno, M.G., Ivy-Ochs, S., Monegato, G., Pini, R., Ravazzi, C., 2015. Stratigraphy of the Ivrea Morainic Amphitheatre (NW Italy). An updated synthesis. Alp. Mediterr. Quat. 28, 29-58.

Gribenski, N., Valla, P.G., Preusser, F., Roattino, T., Crouzet, C., Buoncristiani, J.-F., 2021. Out-of-phase Late Pleistocene glacial maxima in the Western Alps reflect past changes in North Atlantic atmospheric circulation. Geology, 49, 1069-1101. https://doi.org/10.1130/G48688.1.

Gross, G., Kerschner, H., Patzelt, G., 1977. Methodische Untersuchungen über die Schneegrenze in alpinen Gletschergebieten. Z. Gletscherkd. Glazialgeol. 12, 223-251.

Hajdas, I., 2008. Radiocarbon dating and its applications in Quaternary studies. E&G Quat. Sci. J. 57, 2-24. https://doi.org/10.3285/eg.57.1-2.1.

Hajdas, I., Ascough, P., Garnett, M.H., Fallon, S.J., Pearson, C.L., Quarta, G., Spalding, K.L., Yamaguchi, H., Yoneda, M., 2021. Radiocarbon dating. Nat. Rev. Methods Primers 1, 1-26. https://doi.org/10.1038/s43586-021-00058-7.

Hughes, P.D., Woodward, J.C., Van Calsteren, P.C., Thomas, L.E., Adamson, K.R., 2010. Pleistocene ice caps on the coastal mountains of the Adriatic Sea. Quat. Sci. Rev. 29, 3690-3708. https://doi.org/10.1016/j.quascirev.2010.06.032.

Isotta, F.A., Frei, C., Weilguni, V., Perčec Tadić, M., Lassegues, P., Rudolf, B., Pavan, V., Cacciamani, C., Antolini, G. Ratto, S.M., Munari, M., Micheletti, S., Bonati, V., Lussana, C., Ronchi, C., Panettieri, E., Marigo, G., Vertačnik, G., 2014. The climate of daily precipitation in the Alps: development and analysis of a high-resolution grid dataset from pan-Alpine rain-gauge data. Int. J. Climatol. 34, 1657-1675. https://doi.org/10.1002/joc.3794.

Ivy-Ochs, S., Lucchesi, S., Baggio, P., Fioraso, G., Gianotti, F., Monegato, G., Graf, A.A., Akçar, N., Christl, M., Carraro, F., Forno, M.G., Schlüchter, C., 2018. New geomorphological and chronological constraints for glacial deposits in the Rivoli-Avigliana end-moraine system and the lower Susa Valley (Western Alps, NW Italy). J. Quat. Sci. 33, 550-562. https://doi.org/10.1002/jqs.3034.

Jorda, M., Rosique, T., Évin, J., 2000. Données nouvelles sur l'âge du dernier maximum glaciaire dans les Alpes méridionales françaises. C.R. Acad. Sci., Ser. IIa: Sci. Terre Planets 331, 187-193. https://doi.org/10.1016/S1251-8050(00)01408-7.

Kamleitner, S., Ivy-Ochs, S., Monegato, G., Gianotti, F., Akçar, N., Vockenhuber, C., Christl, M., Synal, H.-A., 2022. The Ticino-Toce glacier system (Swiss-Italian Alps) in the framework of the Alpine Last Glacial Maximum. Quat. Sci. Rev. 279, 107400. https://doi.org/10.1016/j.quascirev.2022.107400.

Kelly, M.A., Buoncristiani, J.F., Schlüchter, C., 2004. A reconstruction of the last glacial maximum (LGM) ice-surface geometry in the western Swiss Alps and contiguous Alpine regions in Italy and France. Eclogae Geol. Helv. 97, 57-75. https://doi.org/10.1007/s00015-004-1109-6.

Kerschner, H., Ivy-Ochs, S., 2008. Palaeoclimate from glaciers: Examples from the Eastern Alps during the Alpine Lateglacial and early Holocene. Glob. Planet. Change 60, 58-71. https://doi.org/10.1016/j.gloplacha.2006.07.034.

Kuhlemann, J., Rohling, E.J., Krumrei, I., Kubik, P., Ivy-Ochs, S., Kucera, M., 2008. Regional synthesis of Mediterranean atmospheric circulation during the Last Glacial Maximum. Science 321, 1338-1340. https://doi.org/10.1126/science.1157638.

Kuhlemann, J., Milivojević, M., Krumrei, I., Kubik, P.W., 2009. Last glaciation of the Šara range (Balkan peninsula): increasing dryness from the LGM to the Holocene. Austrian J. Earth Sci. 102, 146-158.

Levenson, Y., Ryb, U., Emmanuel, S., 2017. Comparison of field and laboratory weathering rates in carbonate rocks from an Eastern Mediterranean drainage basin. Earth Planet. Sci. Lett. 465, 176-183. https://doi.org/10.1016/j.epsl.2017.02.031.

Lichtenecker, N., 1938. Die Gegenwärtige und die Eiszeitliche Schneegrenze in den Ostalpen, in: Götzinger, G. (Ed.), Verhandlungen der III Internationalen Quartärkonferenz, INQUA, Vienna, pp. 141-147.

Luetscher, M., Boch, R., Sodemann, H., Spötl, C., Cheng, H., Edwards, R.L., Frisia, S., Hof, F., Müller, W., 2015. North Atlantic storm track changes during the Last Glacial Maximum recorded by Alpine speleothems. Nat. Commun. 6, 1-6. https://doi.org/10.1038/ncomms7344.

Lukas, S., 2006. Morphostratigraphic principles in glacier reconstruction-a perspective from the British Younger Dryas. Prog. Phys. Geogr. 30, 719-736. https://doi.org/10.1177/0309133306071955.

Mattana, U., 1974. Glacialismo e fenomeni periglaciali nel territorio delle Prealpi venete. Nat. Mont. 21, 5-13.

Monegato, G., 2012. Local glaciers in the Julian Prealps (NE Italy) during the last glacial maximum. Alp. Mediterr. Quat. 25, 5-14.

Monegato G., Ravazzi C., Donegana M., Pini R., Calderoni G., Wick L., 2007. Evidence of a two-fold glacial advance during the last glacial maximum in the Tagliamento end moraine system (eastern Alps). Quat. Res. 68, 284-302. https://doi.org/10.1016/j.yqres.2007.07.002.

Monegato, G., Scardia, G., Hajdas, I., Rizzini, F., Piccin, A., 2017. The Alpine LGM in the boreal ice-sheets game. Sci. Rep. 7, 1-8. https://doi.org/10.1038/s41598-017-02148-7.

Nye, J.F., 1952. A method of calculating the thicknesses of the ice-sheets. Nature 169, 529-530. https://doi.org/10.1038/169529a0.

Nye, J.F., 1965. The flow of a glacier in a channel of rectangular, elliptic or parabolic cross-section. J. Glaciol. 5, 661-690. https://doi.org/10.3189/S0022143000018670.

Ohmura, A., Kasser, P., Funk, M., 1992. Climate at the equilibrium line of glaciers. J. Glaciol. 38, 397-411. https://doi.org/10.3189/S0022143000002276.

Ohmura, A., Boettcher, M., 2018. Climate on the equilibrium line altitudes of glaciers: theoretical background behind Ahlmann's P/T diagram. J. Glaciol. 64, 489-505. https://doi.org/10.1017/jog.2018.41.

Oien, R.P., Rea, B.R., Spagnolo, M., Barr, I.D., Bingham, R.G., 2022. Testing the area-altitude balance ratio (AABR) and accumulation-area ratio (AAR) methods of calculating glacier equilibrium-line altitudes. J. Glaciol. 68, 357-368. https://doi.org/10.1017/jog.2021.100.

Osmaston, H., 2005. Estimates of glacier equilibrium line altitudes by the Area× Altitude, the Area× Altitude Balance Ratio and the Area× Altitude Balance Index methods and their validation. Quat. Int. 138, 22-31. https://doi.org/10.1016/j.quaint.2005.02.004.

Pasa, A., 1940. Contributi alla conoscenza dei depositi quaternari della regione veronese. Bollettino del Comitato Glaciologico Italiano, Torino.

Pellegrini, G.B., Albanese, D., Bertoldi, R., Surian, N., 2005. La deglaciazione alpina nel Vallone Bellunese, Alpi meridionali orientali. Geogr. Fis. Dinam. Quat., Suppl. 7, 271-280.

Pellitero, R., Rea, B.R., Spagnolo, M., Bakke, J., Hughes, P., Ivy-Ochs, S., Lukas, S., Ribolini, A., 2015. A GIS tool for automatic calculation of glacier equilibrium-line altitudes. Comput. Geosci. 82, 55-62. https://doi.org/10.1016/j.cageo.2015.05.005.

Pellitero, R., Rea, B.R., Spagnolo, M., Bakke, J., Ivy-Ochs, S., Frew, C.R., Hughes, P., Ribolini, A., Lukas, S., Renssen, H., 2016. GlaRe, a GIS tool to reconstruct the 3D surface of palaeoglaciers. Comput. Geosci. 94, 77-85. https://doi.org/10.1016/j.cageo.2016.06.008.

Penck, A., Brückner, E., 1909. Die Alpen im Eiszeitalter. Tauchnitz, Leipzig.

Pini, R., Furlanetto, G., Vallé, F., Badino, F., Wick, L., Anselmetti, F.S., Bertuletti, P., Fusi, N., Morlock, M.A., Delmonte, B., Harrison, S.P., Maggi, V., Ravazzi, C., 2022. Linking North Atlantic and Alpine Last Glacial Maximum climates via a high-resolution pollen-based subarctic forest steppe record. Quat. Sci. Rev. 294, 107759. https://doi.org/10.1016/j.quascirev.2022.107759.

Provincia di Treviso, ARPAV, 2008. Carta dei suoli della Provincia di Treviso. L.A.C. - Firenze, Firenze.

Ravazzi, C., Badino, F., Marsetti, D., Patera, G., Reimer, P.J., 2012. Glacial to paraglacial history and forest recovery in the Oglio glacier system (Italian Alps) between 26 and 15 ka cal BP. Quat. Sci. Rev. 58, 146-161. https://doi.org/10.1016/j.quascirev.2012.10.017.

Ravazzi, C., Pini, R., Badino, F., De Amicis, M., Londeix, L., Reimer, P.J., 2014. The latest LGM culmination of the Garda Glacier (Italian Alps) and the onset of glacial termination. Age of glacial collapse and vegetation chronosequence. Quat. Sci. Rev. 105, 26-47. https://doi.org/10.1016/j.quascirev.2014.09.014.

Rea, B.R., 2009. Defining modern day Area-Altitude Balance Ratios (AABRs) and their use in glacier-climate reconstructions. Quat. Sci. Rev. 28, 237-248. https://doi.org/10.1016/j.quascirev.2008.10.011.

Rea, B.R., Pellitero, R., Spagnolo, M., Hughes, P., Ivy-Ochs, S., Renssen, H., Ribolini, A., Bakke, J., Lukas, S., Braithwaite, R.J., 2020. Atmospheric circulation over Europe during the Younger Dryas. Sci. Adv. 6, eaba4844. https://doi.org/10.1126/sciadv.aba4844.

Rettig, L., Monegato, G., Mozzi, P., Žebre, M., Casetta, L., Fernetti, M., Colucci, R.R., 2021. The Pleistocene evolution and reconstruction of LGM and Late Glacial paleoglaciers of the Silisia Valley and Mount Raut (Carnic Prealps, NE-Italy). Alp. Mediterr. Quat. 34, 277-290.

Reber, R., Akçar, N., Ivy-Ochs, S., Tikhomirov, D., Burkhalter, R., Zahno, C., Lüthold, A., Kubik, P.W., Vockenhuber, C., Schlüchter, C., 2014. Timing of retreat of the Reuss Glacier (Switzerland) at the end of the Last Glacial Maximum. Swiss J. Geosci. 107, 293-307. https://doi.org/10.1007/s00015-014-0169-5.

Reuther, A.U., Fiebig, M., Ivy-Ochs, S., Kubik, P.W., Reitner, J.M., Jerz, H., Heine, K., 2011. Deglaciation of a large piedmont lobe glacier in comparison with a small mountain glacier – new insight from surface exposure dating. Two studies from SE Germany. E&G Quat. Sci. J. 60, 248-269. https://doi.org/10.3285/eg.60.2-3.03.

Ribolini, A., Spagnolo, M., Cyr, A.J., Federici, P.R., 2022. Last Glacial Maximum and early deglaciation in the Stura Valley, southwestern European Alps. Quat. Sci. Rev. 295, 107770. https://doi.org/10.1016/j.quascirev.2022.107770.

Rossato, S., Monegato, G., Mozzi, P., Cucato, M., Gaudioso, B., Miola, A., 2013. Late Quaternary glaciations and connections to the piedmont plain in the prealpine environment: the middle and lower Astico Valley (NE Italy). Quat. Int. 288, 8-24. https://doi.org/10.1016/j.quaint.2012.03.005.

Rossato, S., Mozzi, P., 2016. Inferring LGM sedimentary and climatic changes in the southern Eastern Alps foreland through the analysis of a 14C ages database (Brenta megafan, Italy). Quat. Sci. Rev. 148, 115-127. https://doi.org/10.1016/j.quascirev.2016.07.013.

Rossato, S., Carraro, A., Monegato, G., Mozzi, P., Tateo, F., 2018. Glacial dynamics in pre-Alpine narrow valleys during the Last Glacial Maximum inferred by lowland fluvial records (northeast Italy). Earth Surf. Dyn. 6, 809-828. https://doi.org/10.5194/esurf-6-809-2018.

Samartin, S., Heiri, O., Kaltenrieder, P., Kühl, N., Tinner, W., 2016. Reconstruction of full glacial environments and summer temperatures from Lago della Costa, a refugial site in Northern Italy. Quat. Sci. Rev. 143, 107-119. https://doi.org/10.1016/j.quascirev.2016.04.005.

Sauro, U., 1973. Il Paesaggio degli alti Lessini. Studio geomorfologico. Museo Civico Storia Naturale di Verona, Memorie fuori serie 6, Verona.

Schilling, D.H., Hollin, J.T., 1981. Numerical reconstructions of valley glaciers and small ice caps, in: Denton, G.H., Hughes, T.J. (Eds.), The Last Great Ice Sheets. Wiley, New York, pp. 207–220.

Seguinot, J., Ivy-Ochs, S., Jouvet, G., Huss, M., Funk, M., Preusser, F., 2018. Modelling last glacial cycle ice dynamics in the Alps. The Cryosphere 12, 3265-3285. https://doi.org/10.5194/tc-12-3265-2018.

Smith, M.J., Rose, J., Booth, S., 2006. Geomorphological mapping of glacial landforms from remotely sensed data: an evaluation of the principal data sources and an assessment of their quality. Geomorphology 76, 148-165. https://doi.org/10.1016/j.geomorph.2005.11.001.

Spagnolo, M., Ribolini, A., 2019. Glacier extent and climate in the Maritime Alps during the Younger Dryas. Palaeogeogr. Palaeoclimatol. Palaeoecol. 536, 109400. https://doi.org/10.1016/j.palaeo.2019.109400.

Spötl, C., Reimer, P.J., Starnberger, R., Reimer, R.W., 2013. A new radiocarbon chronology of Baumkirchen, stratotype for the onset of the Upper Würmian in the Alps. J. Quat. Sci. 28, 552-558. https://doi.org/10.1002/jqs.2645.

Spötl, C., Koltai, G., Jarosch, A.H., Cheng, H., 2021. Increased autumn and winter precipitation during the Last Glacial Maximum in the European Alps. Nat. Commun. 12, 1-9. https://doi.org/10.1038/s41467-021-22090-7.

Synal, H.A., Stocker, M., Suter, M., 2007. MICADAS: a new compact radiocarbon AMS system. Nucl. Instrum. Methods Phys. Res., Sect. B 259, 7-13. https://doi.org/10.1016/j.nimb.2007.01.138.

Taramelli, T., 1875. Dei terreni morenici e alluvionali del Friuli. Annua. Reg. Ist. Tec. Udine 8, 1-91.

Vincenzi, V., Riva, A., Rossetti, S., 2011. Towards a better knowledge of Cansiglio karst system (Italy): results of the first successful groundwater tracer test. Acta Carsologica 40, 147-159. https://doi.org/10.3986/ac.v40i1.34.

Višnjević, V., Herman, F., Prasicek, G., 2020. Climatic patterns over the European Alps during the LGM derived from inversion of the paleo-ice extent. Earth Planet. Sci. Lett. 538, 116185. https://doi.org/10.1016/j.epsl.2020.116185.

Zanferrari, A., Masetti, D., Monegato, G., Poli, M.E., 2013. Geological map and explanatory notes of the Geological Map of Italy at the scale 1:50.000: Sheet 049 “Gemona del Friuli”, ISPRA - Servizio Geologico d’Italia, Rome.

Žebre, M., Sarıkaya, M.A., Stepišnik, U., Yıldırım, C., Çiner, A., 2019. First ^{36}Cl cosmogenic moraine geochronology of the Dinaric mountain karst: Velež and Crvanj Mountains of Bosnia and Herzegovina. Quat. Sci. Rev. 208, 54-75. https://doi.org/10.1016/j.quascirev.2019.02.002.

Žebre, M., Colucci, R.R., Giorgi, F., Glasser, N.F., Racoviteanu, A.E., Del Gobbo, C., 2021. 200 years of equilibrium-line altitude variability across the European Alps (1901-2100). Clim. Dyn. 56, 1183-1201. https://doi.org/10.1007/s00382-020-05525-7.